Activating *PIK3CA* Mutations Induce an Epidermal Growth Factor Receptor (EGFR)/Extracellular Signal-regulated Kinase (ERK) Paracrine Signaling Axis in Basal-like Breast Cancer*⑤

Christian D. Young‡, Lisa J. Zimmerman§‡‡, Daisuke Hoshino¶[e], Luigi Formisano‡, Ariella B. Hanker‡, Michael L. Gatza¶¶, Meghan M. Morrison¶, Preston D. Moore‡, Corbin A. Whitwell‡‡, Bhuvanesh Dave§§, Thomas Stricker‖, Neil E. Bhola‡, Grace O. Silva¶¶, Premal Patel‡, Dana M. Brantley-Sieders‡, Maren Levin[a], Marina Horiates[a], Norma A. Palma[c], Kai Wang[c], Philip J. Stephens[c], Charles M. Perou¶¶, Alissa M. Weaver¶‖, Joyce A. O'Shaughnessy[ab], Jenny C. Chang§§, Ben Ho Park‖‖‖, Daniel C. Liebler§‡‡, Rebecca S. Cook¶**, and Carlos L. Arteaga‡¶**[d]**

Mutations in *PIK3CA*, the gene encoding the p110α catalytic subunit of phosphoinositide 3-kinase (PI3K) have been shown to transform human mammary epithelial cells (MECs). These mutations are present in all breast cancer subtypes, including basal-like breast cancer (BLBC). Using liquid chromatography-tandem mass spectrometry (LC-MS/MS), we identified 72 protein expression changes in human basal-like MECs with knock-in E545K or H1047R *PIK3CA* mutations *versus* isogenic MECs with wild-type *PIK3CA*. Several of these were secreted proteins, cell surface receptors or ECM interacting molecules and were required for growth of *PIK3CA* mutant cells as well as adjacent cells with wild-type *PIK3CA*. The proteins identified by MS were enriched among human BLBC cell lines and pointed to a PI3K-dependent amphiregulin/EGFR/ERK signaling axis that is activated in BLBC. Proteins induced by *PIK3CA* mutations correlated with EGFR signaling and reduced relapse-free survival in BLBC. Treatment with EGFR inhibitors reduced growth of *PIK3CA* mutant BLBC cell lines and murine mammary tumors driven by a *PIK3CA* mutant transgene, all together suggesting that *PIK3CA* mutations promote tumor growth in part by inducing protein changes that activate EGFR. *Molecular & Cellular Proteomics 14: 10.1074/mcp.M115.049783, 1959–1976, 2015.*

PIK3CA[1], the gene encoding the p110α catalytic subunit of phosphatidylinositide-3 kinase (PI3K), is one of the two most

frequently mutated genes in breast cancer. Approximately 80% of these mutations occur in two hot spots in the helical domain (E545K, E542K) and in the catalytic domain (H1047R). *PIK3CA* activating mutations occur in ~40% of luminal and HER2-enriched breast cancer subtypes and ~10% of basal-like breast cancer (BLBC) (1). In this last tumor subtype, mutations in *PIK3CA* are the most frequent activating kinase mutation. Thus, understanding of how *PIK3CA* mutations operate in BLBC is important for identifying therapeutic targets in this subtype of the disease, which lacks approved targeted therapies.

To elucidate mechanisms by which mutant *PIK3CA* transforms MECs, we used immortalized, nontumorigenic MCF10A cells, which exhibit basal-like gene expression. Although MCF10A cells require growth factors for proliferation (2), heterozygous knock-in of E545K or H1047R *PIK3CA* mutation allows growth factor-independent proliferation (3). These knock-in *PIK3CA* mutant MECs provide a robust model in which to study the impact of these mutations without the effects of random insertion and overexpression associated with ectopic gene transduction. Liquid chromatography-tandem mass spectrometry (LC-MS/MS) analysis of these cells identified 72 proteins concordantly altered by both *PIK3CA* mutations. A significant fraction of these were secreted proteins, cell surface receptors or ECM interacting molecules, suggesting *PIK3CA* mutations induce changes involving communication with the tumor microenvironment. This analysis identified a PI3K-induced amphiregulin (AREG)-EGFR-ERK signaling pathway that was required for growth of *PIK3CA*-mutant cells as well as adjacent *PIK3CA*-WT cells. In addition, these protein changes correlated with poor clinical outcome in BLBC. EGFR antagonists inhibited growth of *PIK3CA* mutant BLBC tumors, suggesting a potential therapeutic strategy for patients with this molecular subtype of breast cancer.

EXPERIMENTAL PROCEDURES

Cell Culture, siRNA Transfection, and Virus Production—MCF10A, *PIK3CA* mutant MCF10A (E545K or H1047R), or MCF10AT1 cells were maintained in complete media (DMEM/F12 supplemented with 5% horse serum, 20 ng/ml EGF, 10 μg/ml insulin, 0.5 μg/ml hydrocortisone, 0.1 μg/ml cholera toxin). For experiments under starvation conditions, cells were: (1) seeded in complete media, washed twice with PBS, and then provided with starvation media (DMEM/F12 supplemented with 1% charcoal dextran-treated serum, 10 μg/ml insulin, 0.5 μg/ml hydrocortisone, 0.1 μg/ml cholera toxin) or (2) washed, trypsinized, treated with soybean trypsin inhibitor, and then plated directly in starvation media. Starvation method #2 was employed in proliferation assays assessed by SRB staining to avoid washing and overmanipulating 96-well plates, which disrupts the monolayer and can cause cell death. Parallel plates seeded for lysate collection were seeded in starvation media in the same manner. All breast cancer cells, except SUM102 cells, were maintained in DMEM supplemented with 10% FBS. For experiments in starvation conditions, cells were plated in DMEM supplemented with 1% charcoal dextran-treated serum. SUM102 cells were maintained in complete media (DMEM/F12 supplemented with 5% FBS, 10 μg/ml insulin, 0.5 μg/ml hydrocortisone); for experiments in starvation media, DMEM/F12 supple-mented with 1% charcoal dextran-treated serum, 10 μg/ml insulin, 0.5 μg/ml hydrocortisone was used. When experiments exceeded 3 days, cultures were replenished with fresh media and inhibitors every 3 days. The intrinsic molecular subtype of breast cancer cells used herein and EGFR ligands expression in human breast cancer cell lines are from published microarray data (4). siRNA complexes were prepared at 250 nM in OptiMEM and then diluted tenfold into culture media for a final concentration of 25 nM. For example, 100 μl of 250 nM siRNA were prepared by mixing 1.25 μLof 20 μM siRNA and 1.5 μl Lipofectamine RNAiMAX in a final volume of 100 μl OptiMEM, allowing complexes to form for 15 min and then applying them to cells in 900 μl of starvation media for a final 25 nM siRNA. Amphotropic retroviruses were generated by cotransfecting 2.5 μg proviral plasmid and 2.5 μg pCL-Ampho into 293FT cells using the calcium phosphate method. Lentiviruses were generated by cotransfecting 3.6 μg proviral plasmid, 2.7 μg pΔ8.9 (plasmid encoding *gag*, *pol*, and *rev* genes), and 1.7 μg pVSVG envelope plasmid into 293FT cells using the calcium phosphate method. Packaging cells were fed 24 h post-transfection; virus-containing supernatants were harvested 48 and 72 h post-transfection, diluted 1:4 and applied to target cells with 8 μg/ml polybrene. Target cells were selected with 1 μg/ml puromycin or 500 μg/ml G418 or with flow sorting for mCherry or GFP expression at the Vanderbilt University Flow Cytometry Core Resource.

Reagents—Commercially purchased siRNA, shRNA and antibodies are listed in Table I. pRetroQ-mCherry was provided by Dr. Harold Moses (Vanderbilt University, Nashville, TN). pLNCX2-GFP-Luciferase was provided by Dr. Steven Anderson (University of Colorado, Denver). pLZRS-EphA2-IRES-GFP and pLZRS-GFP were provided by Dr. Jin Chen (Vanderbilt University). Wild type or phosphatase deficient (C1522S) PTPRF in pMT plasmid backbone was provided by Dr. Shuxin Li (Temple University, Philadelphia, PA). Wild type and phosphatase deficient PTPRF open reading frames were amplified by PCR using Elongase polymerase (Life Technologies, Carlsbad, CA) and the following two primers: cctcct*agatct*atggccctgagccagccc and cctcct*agatct*ttacgttgcatagtggtcaaagc (BglII restriction sites are underlined). PCR fragments (~6 kb) were gel extracted and inserted into pCR-XL-TOPO following manufacturer's directions. Full length PTPRF ORFs (wild type and C1522S) were excised from pCR-XL-TOPO using BglII restriction endonuclease and ligated into pMSCV-puro digested with BglII. The wild-type pMSCV-PTPRF failed to express, so a 1.6-kb EcoRI-EcoRI wild-type fragment was inserted into pMSCV-PTPRF (C1522S) and digested with EcoRI to generate wild-type PTPRF in the phosphatase deficient backbone. Sequences were validated by the Sanger method and expression confirmed by immunoblot analysis. Cetuximab was purchased from the Vanderbilt University Medical Center pharmacy. Selumetinib (AZD6244), MK2206 and gefitinib were purchased from Selleck chemicals. BYL719 was provided by Novartis. Recombinant human amphiregulin was purchased from R&D Systems, Minneapolis, MN and resuspended in sterile PBS. Fibronectin coated cell culture plates were purchased from BD Biosciences, Franklin Lakes, NJ.

Mass Spectrometry—Seven replicate 10-cm plates of WT or *PIK3CA* mutant MCF10A cells in starvation media were washed twice with PBS, scraped in PBS and pelleted by centrifugation at 500 × *g* for 5 min. PBS was removed and cell pellets frozen at −80 °C. One pellet was lysed for immunoblot analysis and the other six cell pellets were resuspended for mass spectrometry analysis.

Sample Preparation and Digestion of Cell Pellets—Frozen cell pellets were resuspended 100 μl of trifluoroethanol (TFE) and 100 μl of 100 mM ammonium bicarbonate, pH 8. Samples were sonicated for 20 s followed by 30 s incubation on ice. This sonication step was repeated two additional times making sure samples were placed on ice between sonications. The resulting homogenate was heated with shaking at 1000 rpm for 1 h at 60 °C followed by a second series of

TABLE I
Reagents

siRNA	Vendor	Catalog #
AllStars neg ctrl siRNA	Qiagen	1027281
Universal neg ctrl siRNA	Sigma	SIC001
EphA2 siRNA #6	Qiagen	SI00300188
EphA2 siRNA #12	Qiagen	SI04434990
TGM2 siRNA #1	Qiagen	SI00743715
TGM2 siRNA #5	Qiagen	SI03020927
TGM2 siRNA #6	Qiagen	SI03055465
TGM2 siRNA #7	Qiagen	SI03101966
PXDN siRNA	Sigma	SASI_Hs02_00344041
PXDN siRNA	Sigma	SASI_Hs02_00344042
LAMC2 siRNA	Sigma	SASI_Hs01_00136952
LAMC2 siRNA	Sigma	SASI_Hs01_00136953
LAMB3 siRNA	Sigma	SASI_Hs01_00247331
LAMB3 siRNA	Sigma	SASI_Hs01_00247332
ITGA5 siRNA	Sigma	SASI_Hs01_00058581
ITGA5 siRNA	Sigma	SASI_Hs02_00333426
THBS1 siRNA	Sigma	SASI_Hs01_00148022
THBS1 siRNA	Sigma	SASI_Hs01_00148023
AREG siRNA	Sigma	SASI_Hs01_00014263
AREG siRNA	Sigma	SASI_Hs01_00332258

shRNA	Vendor	Catalog #
TGM2 IPTG induc shRNA	Sigma	TRCN0000272817
PTPRFshRNA	Sigma	TRCN0000002855
PTPRFshRNA	Sigma	TRCN0000002857
non-silencing ctrl shRNA	Sigma	SHC002

Antibody	Vendor	Cat #	Dilution
p110α	Cell Signaling	4249	1:1,000 (immunoblot)
P-S6 (S235/236)	Cell Signaling	4858	1:1,000 (immunoblot)
S6	Cell Signaling	2317	1:1,000 (immunoblot)
P-Akt (S473)	Cell Signaling	9271	1:1,000 (immunoblot)
Akt	Cell Signaling	9272	1:2,000 (immunoblot)
P-ERK (T202/Y204)	Cell Signaling	4370	1:1,000 (immunoblot)
ERK	Cell Signaling	9102	1:2,000 (immunoblot)
Laminin α3	R&D Systems	MAB2144	10 μg/ml (immunofluor)
Laminin β3	Epitomics	7030	1:1,000 (immunoblot)
Laminin β3	Santa Cruz	133178	1:500 (immunoblot)
Laminin γ2	Millipore	MAB19562	1:1,000 (immunoblot)
Fibronectin	Epitomics	1574	1:2,000 (immunoblot)
THBS1	Millipore	BA24	1 μg/ml (immunoblot)
β-Actin	Sigma	A2228	1:10,000 (immunoblot)
EphA2	Millipore	05–480	1:500 (immunoblot)
TGM2	Thermo	Ms-300	1:500 (immunoblot)
Integrin α2	Santa Cruz	6585	1:500 (immunoblot)
Integrin α5	Cell Signaling	4705	1:1,000 (immunoblot)
Integrin α6	Cell Signaling	3750	1:1,000 (immunoblot)
Integrin β1	Cell Signaling	4706	1:1,000 (immunoblot)
Integrin β4	Cell Signaling	4707	1:1,000 (immunoblot)
Vimentin	Cell Signaling	5741	1:1,000 (immunoblot)
PTPRF	R&D Systems	MAB3004	0.5 μg/ml (immunoblot)
CAB39	Cell Signaling	2716	1:1,000 (immunoblot)
Gelsolin	Cell Signaling	8090	1:1,000 (immunoblot)
P-Rb (S780)	Cell Signaling	9307	1:1,000 (immunoblot)
P-EGFR (Y1173)	Santa Cruz	12351	1:500 (immunoblot)
P-EGFR (Y1068)	Cell Signaling	3777	1:1,000 (immunoblot)
P-EGFR (Y1148)	Cell Signaling	4404	1:1,000 (immunoblot)
EGFR	Santa Cruz	03	1:500 (immunoblot)
HER2	Thermo	Rb103	1:1,000 (immunoblot)
P-Tyr	R&D Systems	HAM1676	1:5,000 (immunoblot)
AREG	R&D Systems	AF262	0.5 μg/ml (immunoblot)
AREG	R&D Systems	MAB262	25 μg/ml (neutralize)
mouse IgG	R&D Systems	MAB002	25 μg/ml (neutralize)

sonication steps, as described above (5). Protein quantitation was performed using a BCA protein assay.

An aliquot equivalent to 200 μg was removed and reduced with tris(2-carboxyethyl)phosphine (TCEP, 20 mM) and dithiothreitol (DTT, 50 mM) at 60 °C for 30 min followed by alkylation with iodoacetamide (IAM, 100 mM) in the dark at room temperature for 20 min. The lysate was diluted with the appropriate volume of 50 mM ammonium bicarbonate, pH 8.0, to reduce the TFE concentration to 10%; trypsin was added at a ratio of 1:50 (w:w) and digested overnight at 37 °C. The digested mixture was frozen at -80 °C and lyophilized to dryness. The lyophilized samples were resuspended in 350 μl of HPLC-grade water, vortexed vigorously for 1 min, and desalted using an Oasis HLB 96-well μElution plate (30 μm, 5 mg, Waters Corp., Milford, MA), which were prewashed with 500 μl of acetonitrile and equilibrated with 750 μl of HPLC-grade water. The flow-through was discarded and the plates were washed with 500 μl of HPLC-grade water and the peptides eluted with 80% acetonitrile and dried *in vacuo*. Samples were stored in the freezer until further analysis.

Peptide Fractionation by Isoelectric Focusing (IEF)—Isoelectric focusing (IEF) of tryptic peptides was adapted from the method of Cargile *et al.* (6). Tryptic peptides from 200 μg of protein were resuspended in 155 μl of 6 M urea and loaded in a custom ordered 7 cm, pH 3.5–4.5 ZOOM pH Strips (Invitrogen, Carlsbad, CA) in a ZOOM cassette and allowed to rehydrate for 1 h at room temperature. The loaded strips were focused at 21 °C on a ZOOM IPG Runner system (Invitrogen) using the following program: step at 175 V for 15 min; gradient to 2000 V over 45 min and held at 2000 V for 105 min. The strips were then cut into 15 pieces and placed in separate wells of a 96-well enzyme-linked immunosorbent assay (ELISA) plate. Peptides were eluted from the strips as follows: 200 μl of 0.1% formic acid (FA) for 15 min; 200 μl of 50% acetonitrile (ACN)/0.1% FA for 15 min; 200 μl of 100% ACN/0.1% FA for 15 min. Solutions of extracted peptides were combined and evaporated *in vacuo*, resuspended in 750 μl of 0.1% trifluoroacetic acid, desalted with Oasis HLB 96-well 30 μm μElution plates, (Waters Corp., Milford, MA) and evaporated *in vacuo* with a SpeedVac sample concentrator (ThermoFisher). Peptides were resuspended in 100 μl of 0.1% FA and placed in sample vials for LC-MS/MS analysis.

LC-MS/MS Analysis—Peptide fractions were analyzed on a Thermo LTQ Orbitrap Velos ion trap mass spectrometer equipped with an Eksigent NanoLC 2D pump and AS-1 autosampler. A 2 μl injection volume of peptides was separated on a packed capillary tip (Polymicro Technologies, Phoenix, AZ, 100 μm $\times$ 11 cm) containing Jupiter C18 resin (5 μm, 300 Å, Phenomenex, Torrance, CA) using an in-line solid-phase extraction column (100 μm $\times$ 6 cm) packed with the same C18 resin [using a frit generated with liquid silicate Kasil 1]. Mobile phase A consisted of 0.1% formic acid and Mobile phase B consisted of 0.1% formic acid in acetonitrile. A 95 min gradient was performed with a 15 min washing period (100% A) at a flow-rate of 1.5 μl/min to remove residual salt. Following the washing period, the gradient was increased to 25% B by 50 min, followed by an increase to 90% B by 65 min and held for 9 min before returning to the initial conditions. A full MS scan was collected for peptides from 400–2000 *m/z* on the Orbitrap portion of the instrument at a resolution of 60,000 followed by eight data-dependent MS/MS scans from lowest to highest signal intensity on the LTQ portion. Centroided MS/MS scans were acquired using an isolation width of 3 *m/z*, an activation time of 30 ms, an activation *q* of 0.250 and 35% normalized collision energy. One microscan with a max ion time of 100 ms and 1000 ms was used for each MS/MS and full MS scan, respectively. MS/MS spectra were collected using a dynamic exclusion of 60 s with a repeat of one and repeat duration of one.

Database Searching and Statistical Analysis of Spectral Counts—The .raw files were converted to mzXML files using Scansifter (v2.1.25) under default parameters (7) and are available at MassIVE (massive.ucsd.edu; ID# MSV000079060). These data were searched against the human IPI database (v. 3.56), which contains 76,539 protein entries, using the Myrimatch algorithm (v 1.6.75) (8). The database incorporated both the forward as well as reversed sequences to allow for determination of false discovery rates. The searches were performed allowing a static modification of $+57$ on cysteine (for carboxyamidomethylation from iodoacetamide) and dynamic modifications of $+16$ on methionine (oxidation). Semitryptic peptides were considered in the search parameters. Peptide and fragment ion tolerances were set to $\pm$ 0.01 and 0.5 Da, respectively. A complete detail the search parameters are provided in supplemental Table S4. The data were filtered and assembled with the IDPicker algorithm (v. 3.1.603.0) using a 1% FDR for all peptide-spectrum matches with parsimony applied (minimum protein reporting) and requiring at least two peptides (minimum peptide length of seven amino acids) and three spectra per protein in the entire data set, achieving a final protein-level FDR of 4.6% (9). Spectral count differences between cell lines were analyzed using Quasitel (10), requiring a minimum of 12 total spectral counts across the 12 compared groups and a quasi-*p* value of <0.005.

Orthotopic Tumor Studies—All mice were housed and maintained by the Vanderbilt University Division of Animal Care, an AAALAC-accredited facility in accordance to approved IACUC protocols. Mice were purchase from Harlan laboratories. A MMTV/*rtTA* $\times$ tet-op/*PIK3CA*^{H1047R} mammary tumor was initially harvested from a female transgenic mouse (11, 12) and homogenized in serum-free media with gentleMACS C Tubes (Miltenyi Biotec, Bergisch Gladbach, Germany). Large tissue fragments were removed by brief, low-speed centrifugation with the liquid and smaller tumor fragments transferred to a fresh conical tube that was centrifuged at 200 $\times$ *g*; the tissue pellet was resuspended in 4 ml matrigel diluted with 50% PBS. Tumor homogenates (100 μl) were injected into the inguinal mammary fat pad of $\sim$4-week old female athymic nude mice using a 25-gauge needle and expanded as orthotopic tumors with mice receiving doxycycline (2 mg/ml) *ad libitum* in the drinking water. Mice bearing tumors $\geq$250 mm^3 were randomized to treatment with vehicle (0.5% methylcellulose, 0.1% Tween-80) or gefitinib (100 mg/kg by orogastric gavage, daily). Tumors were measured at the indicated time points and volume calculated by the formula: volume = width^2 $\times$ length/2. When tumor volume exceeded 1 cm^3, mice were sacrificed and tumors harvested 1 h after treatment. Portions of tumors were snap frozen for biochemical analyses or fixed in 10% neutral buffered formalin and embedded in paraffin for histological analyses.

Immunodetection and qPCR—Lysates were generated by removing media from cells, washing monolayers with cold PBS and lysis with RIPA: 50 mM Tris, pH 7.4, 150 mM NaCl, 1% Nonidet P-40, 0.5% Deoxycholate, 0.1% SDS, 1 mM EDTA, 50 mM NaF, 1 mM NaVO$_4$, and 1$\times$ protease inhibitor mixture (Roche). $\sim$30 mg fragments of tumor were minced with surgical scissors in 750 μl lysis buffer [20 mM Tris, pH 7.4, 150 mM NaCl, 1% Nonidet P-40, 10% glycerol, 1 mM EDTA, 1 mM EGTA, 5 mM Na$_4$P$_2$O$_7$, 50 mM NaF, 10 mM β-glycerophosphate, 1 mM Na$_3$VO$_4$ and 1$\times$Protease inhibitor Mixture (Roche)] and lysed with a Polytron rotor-stator homogenizor. Lysates were clarified by centrifugation at 15,000 $\times$ *g* for 15 min. Protein concentration was determined by BCA assay (Thermo scientific). For immunoblot analysis, equal amounts of protein/lane were subjected to SDS-PAGE, transferred to nitrocellulose membranes and analyzed with the antibodies detailed above. For immunofluorescent staining, monolayers grown in chamber slides were fixed with PBS containing 3.7% formaldehyde, washed with PBS, permeabilized with PBS containing 0.25% Triton-X-100, blocked with PBS containing 10% BSA and 0.1% Tween-20, and incubated with primary antibodies diluted in blocking solution overnight. Slides were washed and incubated with

TABLE II
q-RT-PCR primer sets

TGM2 For	CGTGACCAACTACAACTCGG	FN1 For	AGGAAGCCGAGGTTTTAACTG
TGM2 Rev	CATCCACGACTCCACCCAG	FN1 Rev	AGGACGCTCATAAGTGTCACC
PXDN For	AATCAGAGAGATCCAACCTGGG	PTPRF For	ACCATGCTATGTGCCGCAG
PXDN Rev	AATGCTCCACTAGGTATCCTCTT	PTPRF Rev	CCTTGGTCGGATTCCTCACT
ITGB1 For	GTAACCAACCGTAGCAAAGGA	LAMA3 For	CACCGGGATATTTCGGGAATC
ITGB1 Rev	TCCCCTGATCTTAATCGCAAAC	LAMA3 Rev	AGCTGTCGCAATCATCACATT
ITGA5 For	GGCTTCAACTTAGACGCGGAG	LAMB3 For	CCAAAGGTGCGACTGCAATG
ITGA5 Rev	TGGCTGGTATTAGCCTTGGGT	LAMB3 Rev	AGTTCTTGCCTTCGGTGTGG
THBS1 For	TGCTATCACAACGGAGTTCAGT	LAMC2 For	CAAAGGTTCTCTTAGTGCTCGAT
THBS1 Rev	GCAGGACACCTTTTTGCAGATG	LAMC2 Rev	CACTTGGAGTCTAGCAGTCTCT
EPHA2 For	TGGCTCACACACCCGTATG		
EPHA2 Rev	GTCGCCAGACATCACGTTG		

goat-derived alexa fluor 594-conjugated antibodies and mounted with Prolong Gold antifade mounting media (Life technologies). AREG concentration was determined by ELISA (R&D Systems) following the manufacturer's protocol. RNA was purified from cells using RNeasy kit (Qiagen, Valencia, CA) and cDNA was generated using High Capacity cDNA Reverse Transcription Kits (Applied Biosystems, Carlsbad, CA). qPCR was performed with a cDNA equivalent of 50 ng RNA, 1 μM For and Rev primers and SsoAdvanded SYBR Green Supermix (Bio-Rad) following the manufacturer's protocol using a CFX qPCR machine (Bio-Rad). EGFR ligand primers are previously described (13). Other primers, generated with assistance of PrimerBank (14), are listed in Table II. The CT of primer sets for each target gene and Rplp0 or GAPDH were determined in triplicate samples. ΔCT was determined by subtracting the target gene CT from the Rplp0 or GAPDH CT. $2^{\Delta CT}$ was used to determine the expression of each target gene relative to Rplp0 or GAPDH. This relative expression was normalized to control cells.

Proliferation and Invasion Assays—Proliferation assays were performed by plating 1×10^4 cells/60 mm plate in starvation media and replenishing fresh starvation media $\pm$ inhibitors every 2–3 days. Once control plates reached ~75% confluency, plates were fixed and stained with PBS containing 2% formalin, 1% methanol and 0.05% crystal violet, destained with three water rinses, dried, and imaged with a flatbed scanner. Alternatively, 5×10^3 cells/well were seeded in 96-well plates and treated as described with fresh media, conditioned media or drugs replenished every 3 days. At different times, media were decanted and plates were fixed with 10% TCA, washed with tap water, dried, stained with 0.4% sulforhodamine B (SRB), destained with 1% acetic acid, dried, solubilized with 10 mM Tris base and quantitated by spectrophotometric detection at 490 nm using a plate reader. Luciferase activity was detected by incubating cells with 150 μg/ml D-luciferin using an IVIS-200 machine and Living Image software at the Vanderbilt University Institute of Imaging Sciences. For invasion assays, transwell membranes with 8-μm pores (Corning) were coated with matrigel diluted 1:20 in OptiMEM, blocked with 1% BSA and placed in a 24-well plate. Cells (1×10^5) were seeded in starvation media in the upper chamber and allowed to migrate toward DMEM/F12 containing 10% FBS for 24 h. The upper chamber was swabbed to remove cells and the lower chamber was stained/fixed with the above described crystal violet solution and destained with tap water and dried. Photomicrographs (100×) of triplicate membranes were captured, converted to binary images, and the area occupied by cells quantitated using Image J software, summing three photos per membrane. The average area occupied by cells for three membranes was normalized to control cells.

Exosome and Microvesicle Isolation—2.5×10^6 MCF10A cells were plated in duplicate 15-cm dishes in complete medium and allowed to proliferate for 48 h. The monolayers were then washed twice with PBS and each plate incubated with 17 ml serum-free,

EGF-free media for 24 h. Conditioned media was harvested and pooled from each pair of plates (33 ml total); monolayers were trypsinized and cells were counted for normalization of vesicle number to cell number. Conditioned media was centrifuged at 2000 × *g* for 20 min to remove any cells and debris. Eleven ml of conditioned media was kept as "whole conditioned media" and 22 ml were centrifuged at 16,000 × *g* for 30 min. The microvesicle pellet was resuspended in 11 ml serum-free, EGF-free MCF10A media. The 22-ml supernatant was centrifuged at 100,000 × *g* for 20 h; the exosome pellet was resuspended in 11 ml serum-free, EGF-free MCF10A media and the remaining supernatant was considered "vesicle-depleted conditioned media," which was confirmed by Nano Sight vesicle counting. Vesicle number in all fractions was determined by Nano Sight counting and is presented as both vesicle #/cell or vesicle #/ml. Next, 100 μl of each conditioned media/vesicle fraction or unconditioned media was applied to 96-well plates of WT cells in 100 μl starvation media (5×10^3/well) $\pm$ 10 μg/ml cetuximab. Fresh starvation media and whole conditioned media or vesicle fractions were applied on day 2 and 4 and proliferation of WT cells assessed by SRB assay after 7 days of treatment. Fractions were prepared for immunoblot analysis by mixing 300 μl fraction (all in serum-free, EGF-free MCF10A media) with 100 μl 4× sample buffer containing β-mercaptoethanol.

Databases—Kegg analysis of pathways upregulated in *PIK3CA* mutant MCF10A cells was performed using the Duke University GATHER web-based software (15). The intrinsic molecular subtype of breast cancer cells used herein and EGFR ligands expression in human breast cancer cell lines are from published microarray data (4). The EGFR ligand expression in HER2-and $PIK3CA^{H1047R}$ driven mouse mammary tumors are from published microarray data (12). The correlation between gene expression and patient RFS was determined using web-based software, kmplot.com (16). Four EGFR pathway signatures in 476 tumor samples in TCGA data set for which intrinsic subtype by PAM50 and *PIK3CA* mutation status is known (1) were determined by calculating the median score of published EGFR-driven gene lists (17, 18) and then comparing *PIK3CA* mutant to *PIK3CA* WT tumors. EGFR and P-Y1068 EGFR protein abundance was queried from the 361 breast tumors in TCGA RPPA data set (1), comparing *PIK3CA* mutant *versus PIK3CA* WT tumors. *EGFR* transcript abundance was queried from 1031 breast cancer samples in TCGA mRNA sequencing data set as previously described (19) comparing *PIK3CA* mutant to *PIK3CA* WT tumors. To determine if genes corresponding to the proteins upregulated in *PIK3CA* mutant MCF10A cells correlated with BLBC in the TCGA, log transformed TCGA RNAseq gene expression data (1) for 38 genes from 514 tumors were analyzed. Samples were binned into PAM50 basal/claudin-low (94 and 8, respectively) and "other" (230 luminal A, 126 luminal B, and 56 HER2-enriched). Differential expression was quantified by linear model, comparing basal/claudin-low to all other sub-
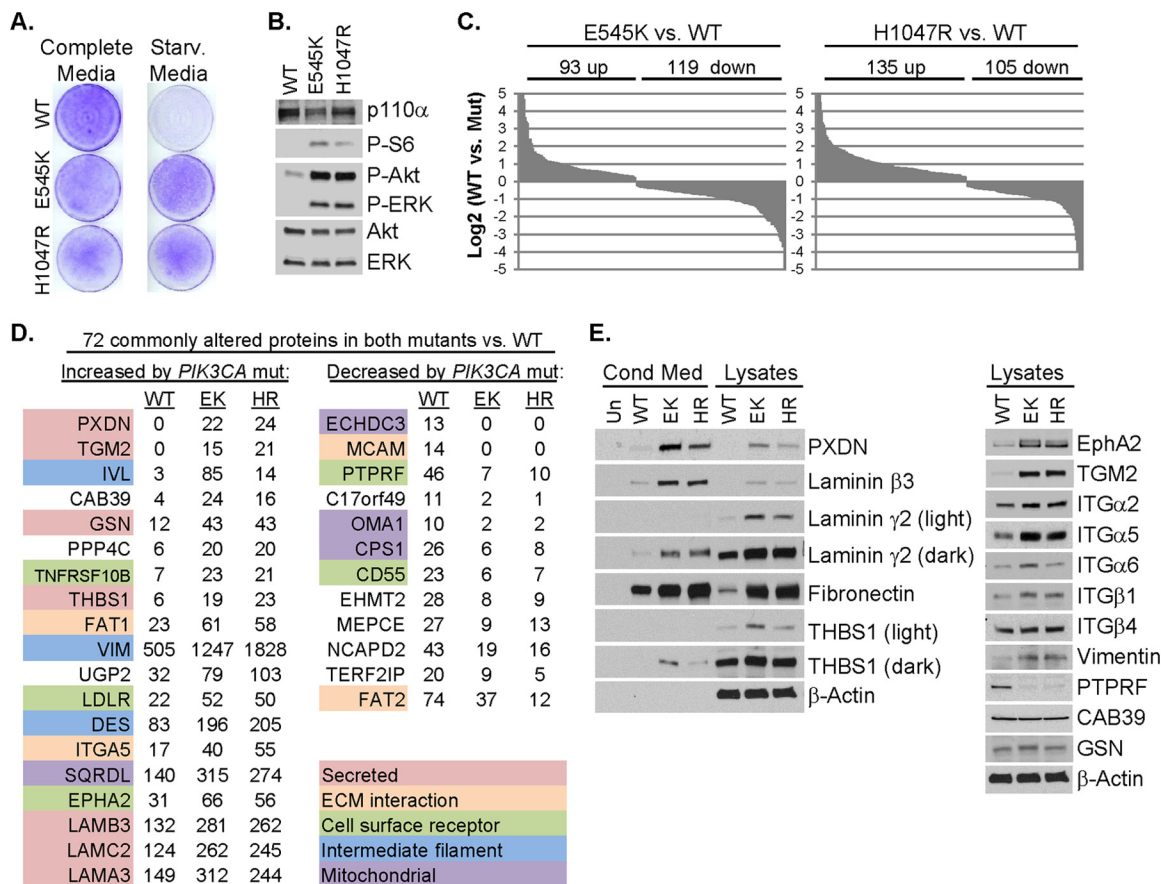
A. Wild type (WT) or *PIK3CA* mutant (E545K or H1047R) MCF10A cells were cultured in complete or starvation media for 6 days; proliferation was assessed by crystal violet staining of cell monolayers.

Fig. 1. Proteomic analysis of *PIK3CA* mutant MCF10A cells shows upregulation of secreted factors and ECM–cell interacting molecules. *A*, Wild type (WT) or *PIK3CA* mutant (E545K or H1047R) MCF10A cells were cultured in complete or starvation media for 6 days; proliferation was assessed by crystal violet staining of cell monolayers. *B*, Lysates of cells cultured for 2 days in starvation media were assessed by immunoblot analysis using the indicated antibodies. *C*, LC-MS/MS analysis of cell lysates was performed to determine relative protein abundance in E545K or H1047R *PIK3CA* MCF10A compared with WT *PIK3CA* MCF10A cells. Each protein which differed between WT and mutant cells with a $p < 0.005$ is presented as the log2 spectral count value of mutant *versus* WT. *D*, Partial list of the most highly up or downregulated proteins common in E545K (EK) and H1047R (HR) MCF10A cells compared with WT MCF10A cells presented as total spectral counts. *E*, Cells were cultured in starvation media. After 48 h, lysates and conditioned media were prepared and subjected to immunoblot analysis with the indicated antibodies.

types. The Bonferroni method was used to correct for multiple hypothesis testing (0.05/38 = 0.0013).

Clinical Trials—ClinicalTrials.gov *Identifier: NCT01097642:* Patients diagnosed with triple negative invasive breast cancer were randomized to preoperative treatment with (1) ixabepilone (4 cycles at 40 mg/m² i.v. every 3 weeks) or (2) ixabepilone + cetuximab (12 weekly infusions, 400 mg/m² i.v. on week 1, then 250 mg/m²). After surgery, pathological complete response was scored in the mastectomy specimen by an expert breast pathologist. DNA was isolated from formalin-fixed, paraffin-embedded diagnostic core biopsies and subjected to competitive allele-specific PCR (Applied Biosystems), testing for E545K or H1047R *PIK3CA* mutations as previously described (20). ClinicalTrials.gov *Identifier: NCT00248287:* Patients with metastatic breast cancer were randomized to receive: 1) Irinotecan (90 mg/m²) + Carboplatin (AUC = 2.0) i.v. on days 1 and 8 of a 21 day cycle or 2) Irinotecan + Carboplatin + Cetuximab (400 mg/m² week 1 and 250 mg/m² weekly thereafter). DNA was extracted from the primary breast tumor and the recurrent lung metastasis and subjected to deep sequencing evaluating 3769 exons of 236 cancer-related genes and 47 introns from 19 genes that are frequently rearranged in cancer

using the Illumina HiSeq 2000 to at an average depth exceeding 500× as previously described (21, 22).

Statistical Analyses—GraphPad Prism or Microsoft Excel was used for statistical analyses. For two-group analyses, Student's t tests were conducted. Error bars represent S.E.

RESULTS

PIK3CA Mutation Increases Secreted Factors and ECM-interacting Proteins—MCF10A cells undergo growth arrest when cultured in media lacking EGF or growth factors (starvation media) (23). However, MCF10A cells with heterozygous knock-in of E545K or H1047R *PIK3CA* mutations exhibit growth factor-independent proliferation and constitutive activation of S6, Akt, and ERK, without altering total levels of p110α (Fig. 1A–1B) (3).

To interrogate how *PIK3CA* mutation alters the proteomic profile of these cells, we performed LC-MS/MS analyses of WT, E545K, and H1047R MCF10A whole cell lysates. This

approach identified differences in 212 and 240 proteins between WT cells and E545K or H1047R cells, respectively (Fig. 1*C* and supplemental Tables S2 and S3). Of these, 72 protein changes were commonly detected in both E545K and H1047R cell lines *versus* WT (43 upregulated and 29 downregulated) [Fig. 1*D* (partial list) and supplemental Table S1]. A complete inventory of proteins identified by LC-MS/MS, including accession number, number of unique peptides identified and percent sequence coverage is provided (supplemental Table S5). Immunoblot analysis was performed to validate a subset of proteins identified by LC-MS/MS. Compared with WT cells, *PIK3CA* mutant cells exhibited increased levels of peroxidasin (PXDN), laminin-332 chains (laminin α3, β3, and γ2), thrombospondin (THBS1), EphA2, tissue transglutaminase (TGM2), integrins β1, α2, α5, and α6, and vimentin (Fig. 1*E*, supplemental Fig. S1*A*). Fibronectin, a primary ligand for integrin α5, was increased in mutant cell lines. Despite increased levels of integrin β4, calcium binding protein 39 (CAB39) and gelsolin (GSN) by LC-MS/MS, immunoblot analysis of these proteins appeared similar in the three cell lines. A receptor tyrosine phosphatase, PTPRF, was decreased in both mutant cell lines. Ten of 11 corresponding mRNA transcripts correlated with changes observed at the protein level (supplemental Fig. S1*B*). Immunoblot analysis of lysates of cells cultured in complete media showed similar expression changes, suggesting these proteomic alterations are not secondary to proliferation induced by mutant *PIK3CA* under growth factor depleted conditions (supplemental Fig. S1*C*).

Of the top 19 proteins upregulated by both *PIK3CA* mutations, seven were secreted proteins and five were cell surface receptors or ECM interacting molecules (Fig. 1*D*). Thus, ~60% of the proteins upregulated by *PIK3CA* mutations may involve communication of mutant cells with their surrounding microenvironment. Furthermore, KEGG pathway analysis showed that *PIK3CA* mutant cells had increased activation of focal adhesion, ECM-receptor interaction and regulation of actin cytoskeleton (supplemental Fig. S1*D*). Consistent with this analysis, PXDN, laminin β3, laminin γ2, fibronectin, and THBS1, but not TGM2, were increased in media conditioned by *PIK3CA* mutant cells (Fig. 1*E*). Also consistent with the alterations in adhesion and actin cytoskeleton-associated molecules, *PIK3CA* mutant cells exhibited an increased ability to invade through matrigel-coated transwell filters (supplemental Fig. S1*E*).

PIK3CA Mutant Cell Proliferation is Reduced Upon Downregulation of Proteins Identified by LC-MS/MS—To assess the functional relevance of the observed protein changes, we transfected WT and *PIK3CA* mutant MCF10A cells with nontargeted siRNA (control) or two siRNAs each targeting EphA2, PXDN, laminin γ2, integrin β1 or TGM2 under starvation conditions. These targets included the most differentially expressed proteins identified by LC-MS/MS (PXDN and TGM2), the receptor tyrosine kinase (RTK) EphA2, one of the three

laminin-332 chains and integrin β1, which functionally dimerizes with all α integrins also identified by LC-MS/MS. Knock-down of EphA2, PXDN, laminin γ2, or integrin β1 resulted in decreased growth factor-independent proliferation of *PIK3CA* mutant cells, without reducing phosphorylation of Akt, suggesting this reduction in cell growth was not because of a blockade of PI3K signaling. ERK phosphorylation was reduced by knock-down of EphA2, but not the other candidates (Fig. 2*A*–2*H*). Because TGM2 expression could not be reduced by siRNA (supplemental Fig. S2*A*), we utilized an IPTG-inducible TGM2 shRNA. shRNA-induced down-regulation of TGM2 did not affect the proliferation of *PIK3CA* mutant cells (supplemental Fig. S2*B*–2*C*). Although decreased EphA2 expression reduced proliferation of *PIK3CA* mutant cells (Fig. 2*G*), EphA2 overexpression in WT cells did not stimulate their proliferation (Fig. 2*I*). Because expression of the PTPRF receptor tyrosine phosphatase was reduced in *PIK3CA* mutant cells, and loss of phosphatases can sustain oncogenic kinase signaling, we next examined whether loss of PTPRF with or without concurrent EphA2 overexpression increased proliferation of WT cells. Loss of PTPRF increased proliferation of WT cells. However, depletion of PTPRF in combination with EphA2 overexpression led to even greater proliferation and ERK phosphorylation, suggesting these two proteins cooperate in promoting growth of *PIK3CA* mutant cells (Fig. 2*I*–2*J*). WT cells expressing PTPRF shRNA showed increased EGFR phosphorylation (Fig. 2*J*), suggesting that the loss of PTPRF in *PIK3CA* mutant cells activates EGFR. Conversely, overexpression of wild-type PTPRF (but not phosphatase-deficient PTPRF) reduced EGFR and ERK phosphorylation and inhibited proliferation of *PIK3CA^{H1047R}* cells (Fig. 2*K*–2*L*). These data suggest that, in addition to Akt, *PIK3CA* mutation activates other signaling pathways that drive cell proliferation.

Secreted Factors from PIK3CA Mutant Cells Activate EGFR/ERK and Promote Growth Factor- and PI3K-Independent Proliferation—Media conditioned by *PIK3CA* mutant cells markedly increased proliferation, P-Rb and P-ERK in recipient WT cells. All these responses were blocked by the MEK1/2 inhibitor AZD6244 (selumetinib) (24) but not by the p110α-specific inhibitor BYL719 (25) (Fig. 3*A*–*B*), suggesting a MEK-dependent paracrine effect of the mutant cells on the WT cells. Both AZD6244 and BYL719 inhibited proliferation and P-Rb levels in *PIK3CA* mutant cells (Fig. 3*C*–3*D*). To investigate this paracrine effect further, we cocultured 1000 GFP-luciferase expressing WT MCF10A cells with 500, 250, 125, or 62 mCherry-labeled WT, E545K or H1047R cells. Photomicrographs captured at the end of 2 weeks in starvation media showed expansion of WT-GFP+ cells when cocultured with *PIK3CA* mutant-mCherry cells, but not with WT-mCherry cells (Fig. 3*E*). Using luciferase activity to measure WT cell number, we found increased luminescence of WT-GFP-luciferase cells cocultured with *PIK3CA* mutant mCherry but not with WT-mCherry cells (Fig. 3*F*).
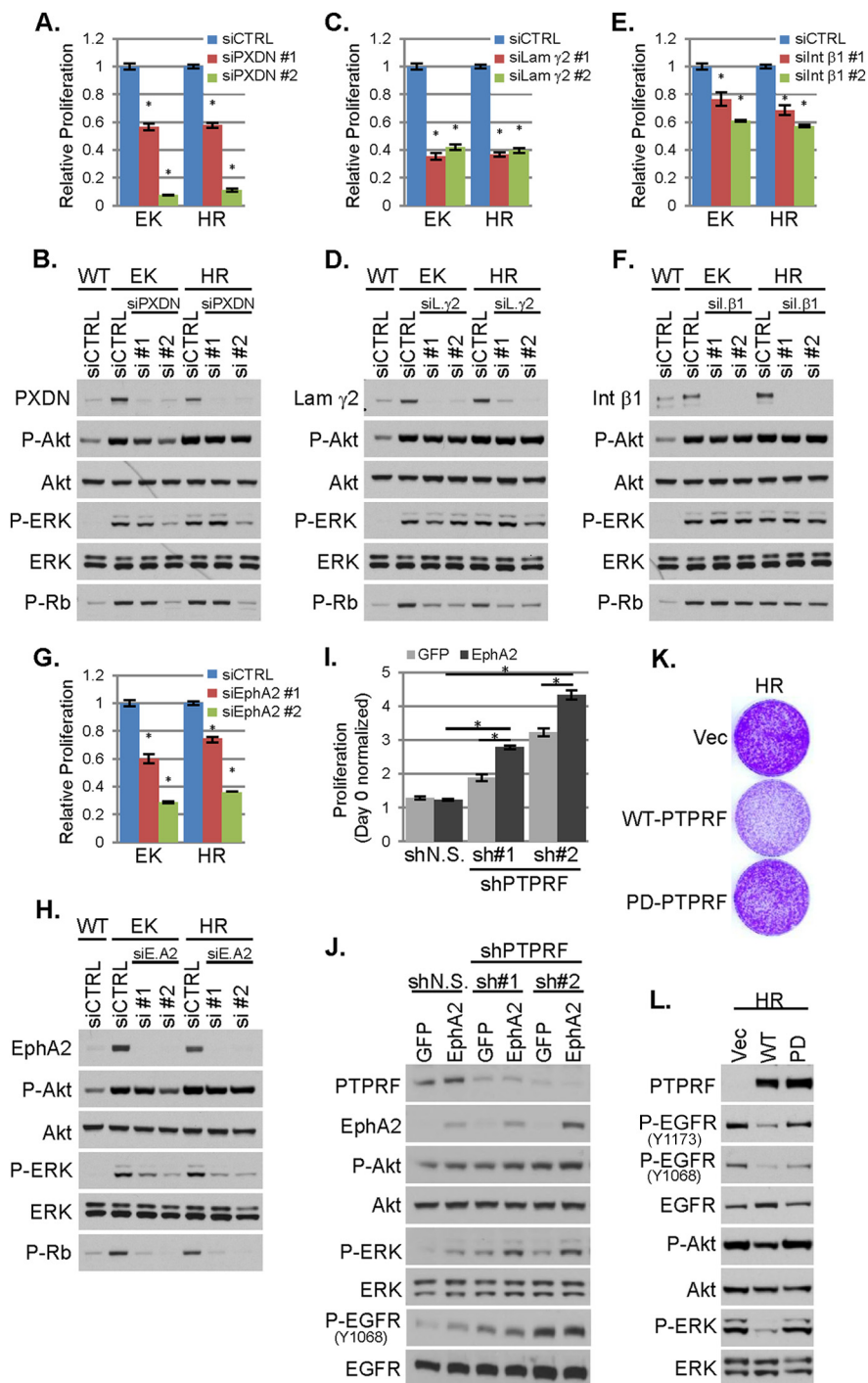
FIG. 2. **Loss of PTPRF and upregulation of EphA2 cooperate to promote EGF-independent proliferation and EGFR activation.** WT or *PIK3CA* mutant (EK or HR) MCF10A cells were transfected with 25 nM control siRNA or two different siRNA sequences targeting PXDN, *A–B*, Laminin γ2, *C–D*, Integrin β1, *E–F*, or EphA2, *G–H*, in starvation media. *A, C, E, G*, Relative proliferation, normalized to control siRNA transfected cells, was assessed at 96 h by SRB assay (average of six biological replicates ± S.E.). *B, D, F, H*, Cells were harvested 48 h after transfection and cell lysates evaluated by immunoblot analysis with the indicated antibodies. *I*, Proliferation of WT MCF10A cells stably expressing GFP or EphA2 and nonsilencing shRNA (shN.S.) or PTPRF-targeted shRNA (sh#1 or sh#2) was determined by SRB assay after 5 days of culture in starvation media (average of six biological replicates ± S.E.). *J*, Cells treated as described in panel I were lysed after 3 days and evaluated by immunoblot analysis. *K*, *PIK3CA^{H1047R}* (HR) MCF10A cells stably expressing empty vector (vec), wild type (WT) PTPRF, or phosphatase-deficient (PD) PTPRF were seeded in equal numbers and cultured for 9 days in starvation media (with media replenished every 3 days); proliferation was assessed by crystal violet staining of cell monolayers. *L*, Cells treated as described in panel K were harvested after 3 days of culture and lysates evaluated by immunoblot analysis with the indicated antibodies. *p < 0.05 Student's *t* test.
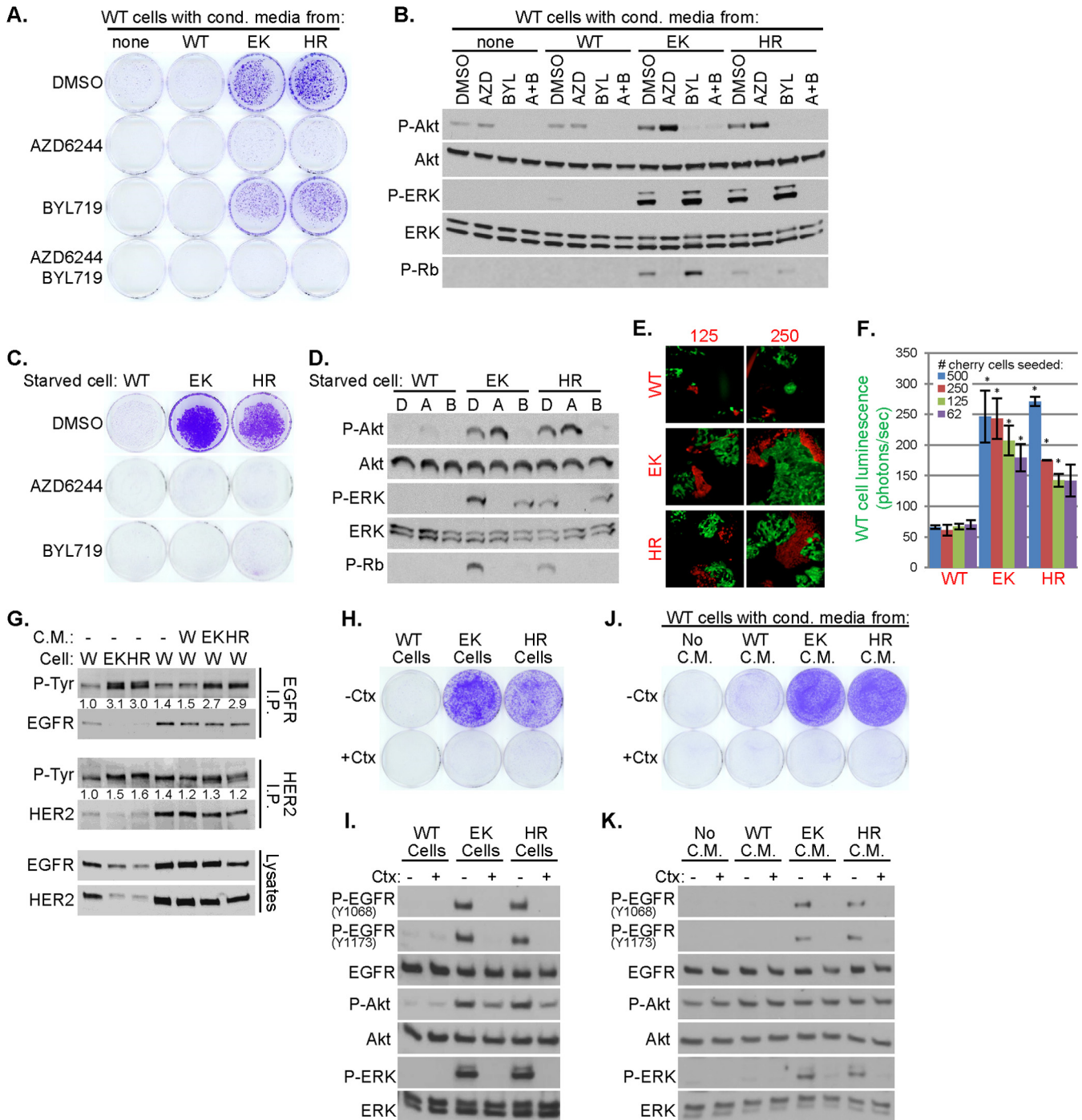
FIG. 3. **Secreted factors from *PIK3CA* mutant MCF10A cells are sufficient to promote growth factor- and p110α-independent proliferation and EGFR activation.** *A–B*, WT MCF10A cells in starvation media were treated with conditioned media harvested from WT or *PIK3CA* mutant (EK or HR) cells and DMSO, 1 μM AZD6244 or 1 μM BYL719. Cell proliferation was assessed by staining monolayers with crystal violet on day 18, *A*. After 5 days, lysates were prepared and evaluated by immunoblot analysis, *B*. *C–D*, WT or *PIK3CA* mutant MCF10A cells were cultured in starvation media in the presence of DMSO, 1 μM AZD6244 or 1 μM BYL719. Proliferation was assessed after 8 days, *C*. After 24 h, lysates were prepared for immunoblot analysis, *D*. *E–F*, One-thousand WT GFP-luciferase-expressing MCF10A cells were incubated in starvation media with 62, 125, 250, or 500 mCherry labeled WT, EK, or HR MCF10A cells. Cells were cultured for 14 days before being photomicrographed, *E*, or imaged with an IVIS200 bioimager, *F*, to quantitate luciferase expression (average photons/sec of biological duplicates ± S.E.; *$p < 0.05$ Student's *t* test). *G*, WT (W), E545K (EK) or H1047R (HR) MCF10A cells were cultured in starvation media for 2 days (lanes 1–3); WT cells were treated with the indicated conditioned media for 7 days (lanes 4–7). Cell lysates were harvested and subjected to immunoprecipitation and P-Tyr immunoblot analysis. P-Tyr band intensities were quantitated and normalized to lane 1. *H–I*, WT, EK, or HR

PIK3CA mutant cells or WT cells treated with media conditioned by *PIK3CA* mutant cells showed increased EGFR phosphorylation compared with untreated WT cells, whereas phosphorylation of the closely related HER2 RTK was unaffected (Fig. 3*G*). The EGFR blocking antibody cetuximab reduced P-ERK and proliferation in *PIK3CA* mutant cells (Fig. 3*H*–3*I*). The induction of proliferation, P-EGFR and P-ERK in WT cells treated with the media conditioned by *PIK3CA* mutant cells was also inhibited by cetuximab (Fig. 3*J*–3*K*). These data suggest that *PIK3CA* mutation induces EGFR- and MEK-dependent paracrine signals that drive cell growth independent of intrinsic PI3K activity in the recipient cell population.

Amphiregulin Induced by PIK3CA Mutations is Necessary and Sufficient to Promote Growth Factor-Independent Proliferation—Because EGFR-activating ligands were not identified in the MS analysis, we performed quantitative PCR analysis measuring all eight ErbB family ligands. This revealed increased levels of transcripts encoding HB-EGF, epiregulin (EREG) and amphiregulin (AREG) in *PIK3CA* mutant cells. Compared with WT cells, *PIK3CA* mutant cells contained >10-fold and fourfold higher AREG mRNA and protein, respectively (Fig. 4*A*–4*B*). Increased expression of AREG in *PIK3CA* mutant *versus* WT cells was observed in both complete media and starvation media, suggesting AREG overexpression is not secondary to increased cell proliferation induced by the *PIK3CA* mutations (supplemental Fig. S3*A*). Interrogation of cDNA microarray data for five EGFR ligands in 51 human breast cancer cell lines (4) showed that *AREG* expression is increased in *PIK3CA* mutant compared with *PIK3CA* WT cells, whereas the other four ligands are similarly expressed (supplemental Fig. S3*B*). AREG protein expression also correlated with *PIK3CA* mutation status in a panel of 19 breast cancer cell lines: four of the top five AREG expressing cells contained *PIK3CA* hot spot mutations (supplemental Fig. S3*C*). Inhibition of p110α with BYL719 decreased AREG transcript and protein expression in *PIK3CA* mutant MCF10A cells (Fig. 4*C*–4*D*). Treatment with the Akt inhibitor MK-2206 (26) also suppressed AREG protein in *PIK3CA* mutant cells (supplemental Fig. S3*D*). Finally, inhibition of p110α with BYL719 decreased AREG protein levels in *PIK3CA* mutant MCF7, T47D, BT20, and SUM102 breast cancer cells (supplemental Fig. S3*E*–S3*F*), further supporting a causal association between PI3K/Akt signaling and AREG expression.

Similar to *PIK3CA* mutant cells, MCF10AT1 cells, which bear a G12V *HRAS* mutation, proliferate in the absence of exogenous growth factors (supplemental Fig. S3*G*). We treated WT, *PIK3CA* mutant or *HRAS* mutant MCF10A cells with IgG or an AREG neutralizing monoclonal antibody (27) in growth factor-depleted media. Treatment with the AREG antibody decreased P-EGFR, P-ERK and proliferation in *PIK3CA* mutant but not in *HRAS* mutant MCF10AT1 cells (Fig. 4*E*–4*F*). AREG siRNA also decreased proliferation, P-Rb and P-ERK in *PIK3CA* mutant cells (supplemental Fig. S3*H*–S3*I*). Finally, antibody-mediated AREG blockade reduced the proliferation of WT cells induced by media conditioned by *PIK3CA* mutant cells (Fig. 4*G*). Taken together, these results suggest the induction of AREG is specific to a mutant *PIK3CA*. Serum- and growth factor-starved WT cells treated with AREG (5 ng/ml) transiently increased EGFR phosphorylation at Y1068 and Y1173. However, AREG-induced ERK activation was maintained through 48 h (supplemental Fig. S3*J*). These data suggest that AREG-induced EGFR phosphorylation is relatively transient, but results in sustained activation of downstream signal transducers such as ERK.

HRAS mutant MCF10AT1 cells displayed increased activation of Akt, ERK and S6, increased expression of PXDN, THBS1 and EphA2, and decreased PTPRF expression compared with WT cells. However, unlike *PIK3CA* mutant cells, *HRAS*^{G12V} cells did not overexpress laminin β3, laminin γ2, fibronectin, TGM2, integrin α5 or integrin β1 (supplemental Fig. S4*A*), and secreted three to sevenfold less AREG than *PIK3CA* mutant cells (supplemental Fig. S4*B*). Further, media conditioned by *PIK3CA* mutant cells but not by *HRAS* mutant cells, stimulated proliferation of WT cells (supplemental Fig. S4*C*), suggesting that induction of these proteins involved in paracrine and/or microenvironment interactions may be specific to *PIK3CA* mutations.

The media conditioned by *PIK3CA* mutant cells contained ~150–300 pg/ml AREG (supplemental Fig. S4*B*). However, ≥2500 pg/ml of recombinant AREG was required to stimulate WT cell proliferation and P-ERK (supplemental Fig. S4*C*–S4*D*) suggesting that, in addition to AREG, other factors contribute to the growth promoting effects of *PIK3CA* mutant conditioned media. For example, fibronectin, which is robustly secreted by *PIK3CA* mutant cells but not by *HRAS* mutant cells (Fig. 1*E*, supplemental Fig. S4*A*), enhanced AREG-induced proliferation and P-ERK in WT cells without altering P-Akt or P-EGFR (Fig. 4*H*–4*I*). Additionally, fibronectin induced TGM2 expression while AREG induced EphA2, THBS1, and fibronectin expression in WT cells (supplemental Fig. S4*E*). These results suggest AREG and fibronectin secreted by *PIK3CA* mutant cells exert additive and temporally distinct paracrine effects and also induce expression of some of the proteins modulated by mutant *PIK3CA* that were identified by LC-MS/MS.

AREG and ECM proteins have been shown to be carried on exosomes, late endosome-derived extracellular vesicles that contains bioactive protein and RNA cargoes (28, 29).

MCF10A cells were cultured in starvation media ±10 μg/ml cetuximab. Cell proliferation was assessed after 8 days, *H*, and cell lysates prepared for immunoblot analysis after 2 days, *I*. *J*–*K*, Starvation media conditioned by WT, EK, or HR MCF10A cells were applied to WT MCF10A cells plated in starvation media ±10 μg/ml cetuximab. Cell proliferation was assessed after 8 days, *J*, and cell lysates prepared for immunoblot analysis after 2 days, *K*. Media and drugs were replenished every 3 days in all experiments.
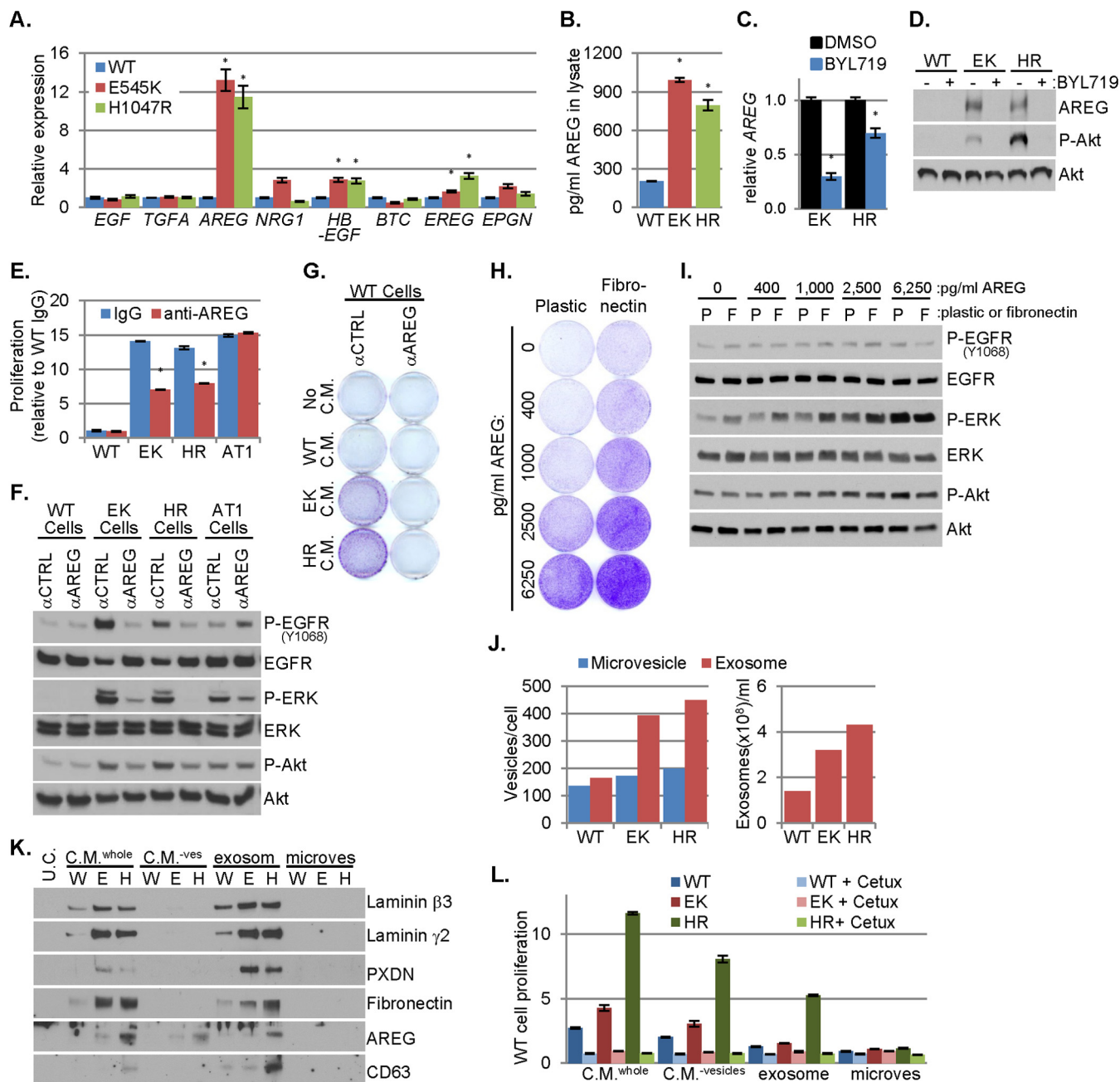
FIG. 4. **Amphiregulin induced by *PIK3CA* mutation promotes EGF-independent cell proliferation.** *A*, The expression of eight EGFR-family ligands in WT and *PIK3CA* mutant MCF10A cells cultured in starvation media was determined by qPCR and normalized to the expression of *RPLP0*; the normalized expression of each ligand in each mutant cell line is presented relative to WT cells (average of biological quadruplicates ± S.E.). *B*, Amphiregulin (AREG) concentration in 25 µg of WT or *PIK3CA* mutant MCF10A cell lysate was determined by ELISA (average of technical duplicates ± S.E.). Lysates were harvested from cells cultured in starvation media. *C–D*, WT or *PIK3CA* mutant MCF10A cells were cultured in starvation media containing DMSO or 1 µM BYL719. *C*, After 48 h, RNA was harvested and qPCR was used to determine the *RPLP0* normalized expression of *AREG* in each mutant cell line, presented relative to the DMSO control (average of biological triplicates ± S.E.). *D*, After 72 h, cell lysates were prepared and analyzed by immunoblot analysis with the indicated antibodies. *E–F*, WT, *PIK3CA* mutant (EK and HR), or *HRAS* mutant (AT1) MCF10A cells were cultured in starvation media containing 25 µg/ml mouse IgG or AREG neutralizing antibody. Relative proliferation was assessed by SRB assay after 6 days of treatment (*E*; average of biological triplicates ± S.E.) and lysates were prepared for immunoblot analysis after 2 days, *F*. *G*, Starvation media conditioned by WT, EK or HR MCF10A cells were applied to WT MCF10A cells cultured in starvation media containing 25 µg/ml mouse IgG or AREG neutralizing antibody. After 9 days, monolayers were stained with crystal violet to assess cell proliferation. *H–I*, Growth factor starved WT MCF10A cells were seeded to plastic or fibronectin-coated plates and treated with the indicated doses of AREG. After 7 days, proliferation was assessed by crystal violet staining, *H*. Lysates were prepared for immunoblot analysis after 3 days, *I*. *J*, The number of microvesicles or exosomes harvested from starvation media conditioned

We previously reported that exogenous expression of *PIK3CA*[H1047R] promotes exosome secretion in head and neck cancer cells (30). To test this in knock-in *PIK3CA* mutant MECs, we purified exosomes and larger shed microvesicles from conditioned media. *PIK3CA* mutant cells secreted nearly 3-fold more exosomes as WT cells, whereas microvesicle secretion was relatively unaltered (Fig. 4*J*). Laminin β3, laminin γ2, PXDN, fibronectin, and the exosome marker CD63 were present in whole conditioned media and exosome fractions, but were not detected in the microvesicle fraction or in conditioned media depleted of vesicles, suggesting that these proteins are mainly associated with secreted exosomes. AREG was detected in whole conditioned media, conditioned media depleted of vesicles, and in the exosome fraction (Fig. 4*K*), suggesting that AREG is secreted on exosomes and shed either from the exosome or plasma membrane surfaces by proteinases (31). *PIK3CA* mutant fractions contained more AREG than *PIK3CA* WT fractions, and H1047R cells contained more AREG than E545K cells. The fractions with highest AREG induced the greatest proliferation of WT cells. Additionally, whole conditioned media contained more AREG and conferred greater proliferation than the other fractions (Fig. 4*K*–4*L*). The proliferation conferred by all fractions was blocked by treatment with cetuximab (Fig. 4*L*). These data suggest enhanced exosome secretion induced by mutant *PIK3CA* provides an EGFR-dependent mechanism for the delivery of secreted factors associated with transforming potential.

Proteins Induced by PIK3CA Mutations Correlate With Decreased Relapse-free Survival (RFS) and EGFR Signaling in BLBC—Using a panel of luminal and BLBC cell lines, we interrogated expression of proteins found by MS to be altered in *PIK3CA* mutant MCF10A cells. Of these, TGM2, EphA2, integrin β1, integrin α5, fibronectin, THBS1, laminin β3, and laminin γ2 were also overexpressed in basal-like compared with luminal breast cancer cell lines (Fig. 5*A*, supplemental Fig. S5*A*). PTPRF, which is down-regulated in *PIK3CA* mutant MCF10A cells, is reduced in BLBC cell lines. However, there was no correlation of these changes with *PIK3CA* mutation status, suggesting the possibility that the suite of proteins altered in *PIK3CA* mutant MCF10A cells is more specific to the BLBC subtype of breast cancer. Further, in primary breast tumors in the TCGA, mRNAs of 18/38 proteins upregulated in *PIK3CA* mutant cells were also enriched in BLBC, 8/38 were enriched in nonbasal cancers (HER2 and luminal), and the remaining 12 were not associated with any subtype (supplemental Fig. S5*B*).

We next interrogated public data sets (16) to correlate transcript expression of the proteins enriched in BLBC cell lines with breast cancer patient outcome. High expression of *PXDN* or *THBS1* correlated with a shorter RFS in BLBC (relapse hazard ratios of 1.52 and 1.34, respectively), but not when all breast cancer subtypes were analyzed together. High expression of *EPHA2*, *LAMA3*, *LAMB3*, and *LAMC2* each correlated with better RFS when all breast cancer subtypes were analyzed jointly. This correlation with an improved RFS was lost in BLBC (Fig. 5*B*, supplemental Fig. S5*C*). In examining multiple genes, combined high expression of PXDN, THBS1, integrin α5, EphA2, laminin α3, laminin β3, and laminin γ2 correlated with shorter RFS in BLBC (relapse hazard ratio of 1.85), but had no prognostic value when applied to all breast cancers (hazard ratio of 1.05) (Fig. 5*C*), further implying a subtype specific association.

Next, to determine whether these proteins play a role in BLBC growth, we transfected four BLBC cell lines with siRNAs targeting PXDN, THBS1, EphA2, laminin γ2, laminin β3, or integrin α5. All four cell lines exhibited reduced proliferation when PXDN or THBS1 expression was knocked down, whereas three of the four cell lines were at least modestly sensitive to reduction of laminin β3 or integrin α5 (Fig. 5*D*, supplemental Fig. S5*D*). The proliferation of a luminal cell line, MDA-MB-361, which has low expression of these proteins, was not inhibited by these siRNAs, with the exception of PXDN knockdown. These data suggest that the proteins identified by LC-MS/MS of *PIK3CA* mutant MCF10A cells are associated with the virulence of BLBC.

Analysis of the breast tumor reverse phase protein array (RPPA) data in TCGA (1) showed that *PIK3CA* mutant BLBCs display increased levels of EGFR and P-Y1068-EGFR compared with *PIK3CA* WT BLBCs. However, neither EGFR nor P-Y1068-EGFR correlated with *PIK3CA* status when all breast cancers were examined jointly (Fig. 6*A*). Similarly, *EGFR* gene expression was higher in *PIK3CA* mutant BLBC than *PIK3CA* WT BLBC. There was no difference in *EGFR* expression between *PIK3CA* mutant and WT when all breast cancer subtypes were evaluated together (Fig. 6*B*). TCGA gene expression data were used to compute published EGFR pathway activation scores (17, 18) comparing *PIK3CA* WT and mutant breast cancers. Two of four EGFR activation scores were increased in *PIK3CA* mutant BLBCs compared with WT. However, when all breast cancer subtypes were jointly evaluated, none of the EGFR pathway scores was higher in *PIK3CA* mutant cancers (Fig. 6*C*). These data suggest *PIK3CA* muta-

---

by WT or *PIK3CA* mutant MCF10A cells was determined by Nano Sight and normalized to the number of cells (left) or to volume (right). *K*–*L*, Unconditioned starvation media (U.C.), whole conditioned media (C.M.[whole]), conditioned media depleted of vesicles (C.M.[−ves]), and exosome fraction or microvesicle fraction were evaluated by immunoblot analysis with the indicated antibodies, *K*. WT MCF10A cells plated in starvation media were treated with these fractions ±10 μg/ml cetuximab; proliferation was assessed by SRB assay after 7 days in culture (*L*; average of six biological replicates ± S.E.). Media and drugs were replenished every 3 days in all experiments. *$p < 0.05$ Student's *t* test.
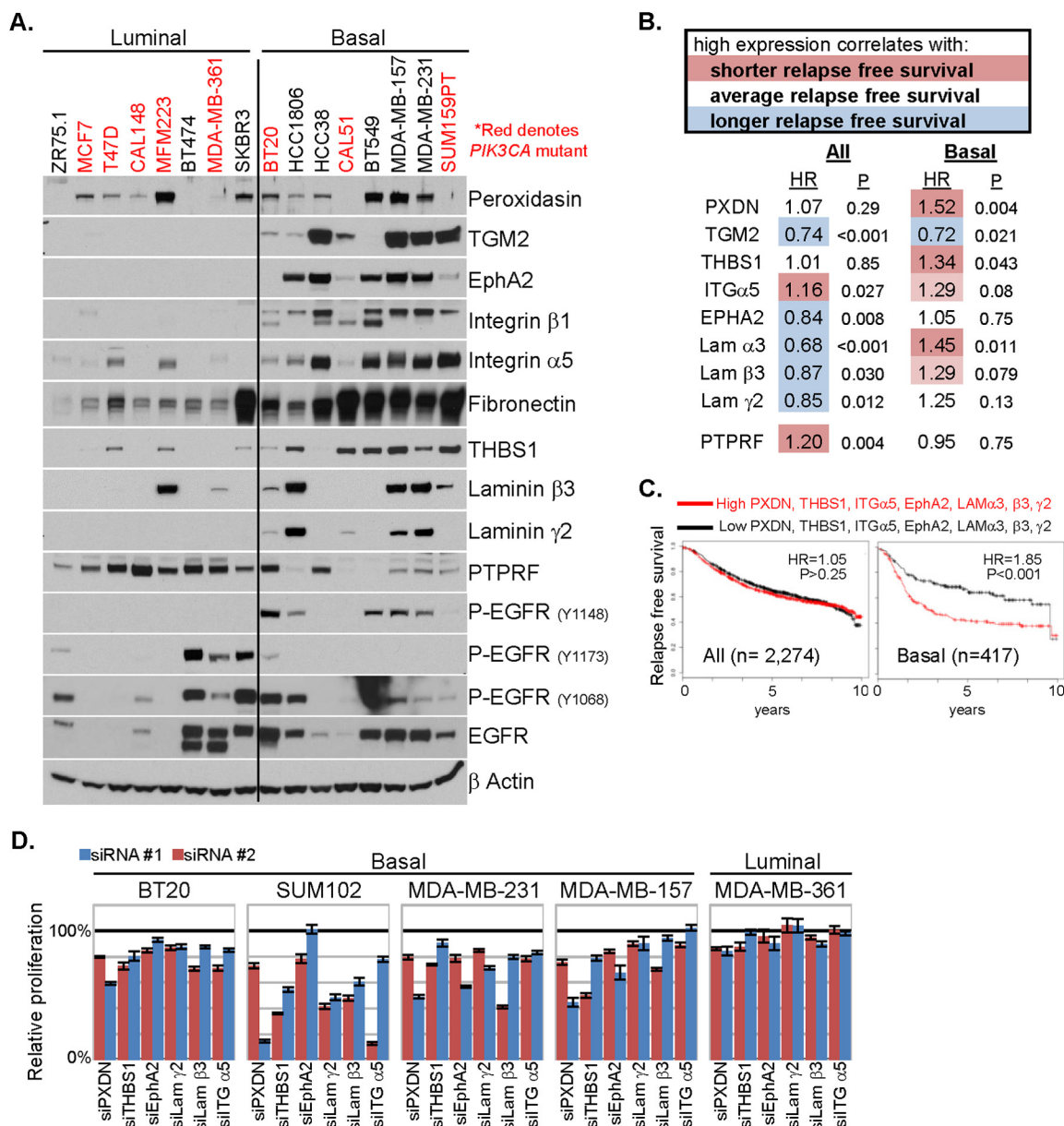
FIG. 5. **Proteins upregulated by *PIK3CA* mutation correlate with decreased relapse free survival in BLBC.** *A*, Lysates of a panel of luminal and BLBC cell lines were prepared and evaluated by immunoblot analysis with the indicated antibodies. *B*, A data set that includes RFS time and cDNA gene expression profiling data of the tumors from 2274 breast cancer patients (all) or a subset of 417 BLBC was queried (16). For each of the indicated genes, groups were divided equally in half (high expressors and low expressors); the RFS hazard ratio (HR) attributed to high expression and logrank *p* value between the two groups are presented. *C*, The same data set was queried with a multiple comparison of high *versus* low expression of the seven indicated genes. The Kaplan-Meier survival plots, hazard ratio and logrank *p* values for all patients and patients with BLBC are presented. *D*, The five indicated cell lines were transfected with control siRNA or two different siRNA sequences targeting PXDN, THBS1, EphA2, laminin γ2, laminin β3, or integrin α5 at a siRNA concentration of 25 nM in complete media. Relative proliferation, normalized to control siRNA transfected cells, was assessed at 96 h by SRB assay (average of five biological replicates ± S.E.).

tion is correlated with EGFR activity only in BLBC but not the other molecular subtypes of breast cancer.

Clinical Activity of EGFR Inhibitor against PIK3CA Mutant Breast Cancers—EGFR is overexpressed in the majority of patients with triple negative breast cancer (TNBC). This clinical subtype of breast cancer predominantly exhibits basal-like

gene expression (1). Clinical trials with EGFR inhibitors have been performed in patients with TNBC. In a study of patients with metastatic TNBC, a doubling of the response rate was observed when cetuximab was combined with cisplatin compared with cisplatin alone (32). In a neoadjuvant trial of ixabepilone and cetuximab (ClinicalTrials.gov #NCT01097642),
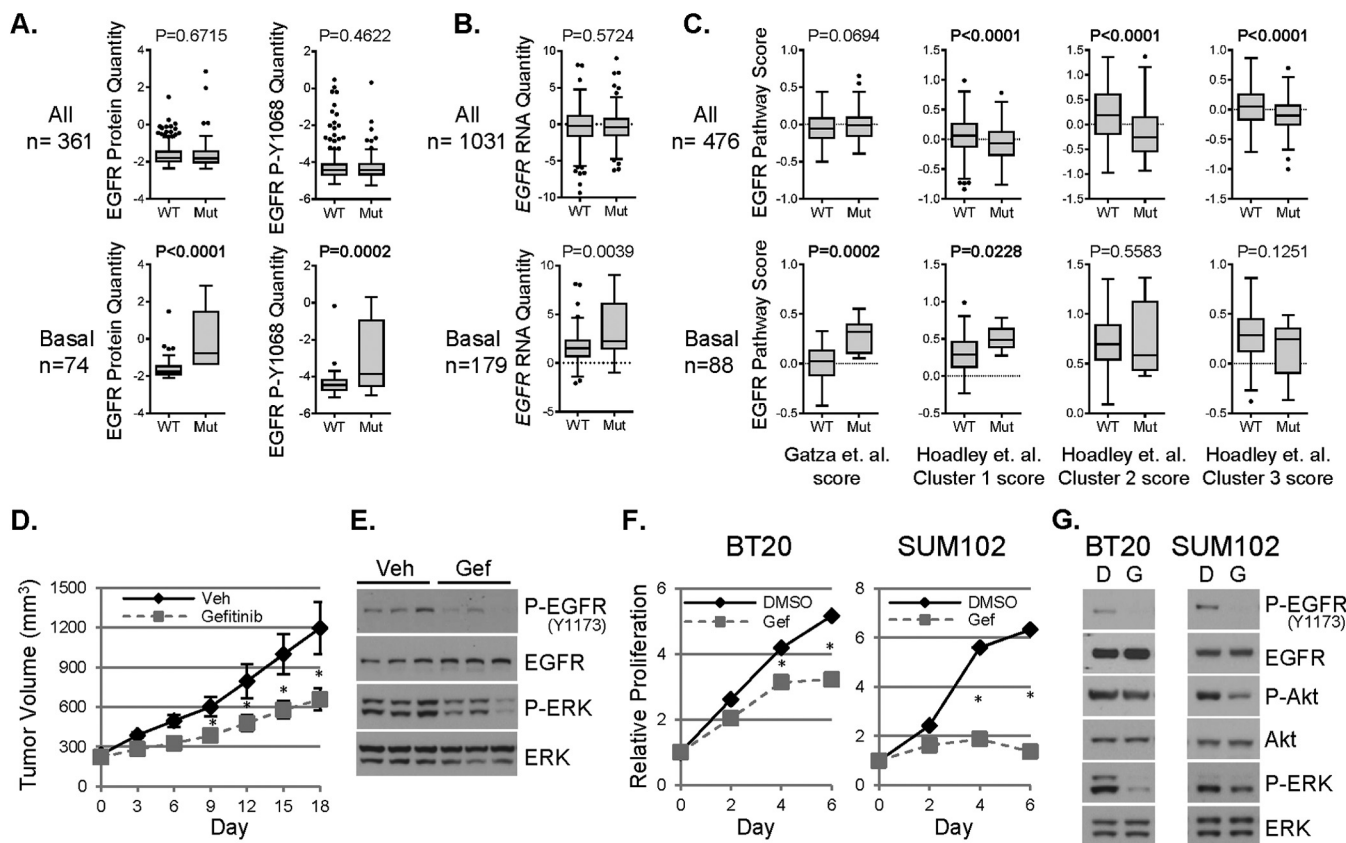
FIG. 6. ***PIK3CA* mutations correlate with EGFR activity in basal-like breast cancer.** *A*, TCGA reverse phase protein array data were analyzed to determine EGFR and P-Y1068 EGFR levels comparing *PIK3CA* WT *versus PIK3CA* mutant tumors in all breast cancers (top) or in the basal-like subtype (bottom). *B*, TCGA gene expression data were analyzed to determine *EGFR* levels comparing *PIK3CA* WT *versus PIK3CA* mutant tumors in all breast cancers (top) or in the basal-like subtype (bottom). *C*, TCGA gene expression data was used to compute four different EGFR pathway scores (17, 18) comparing *PIK3CA* WT to *PIK3CA* mutant tumors in all breast cancers (top) or in the basal-like subtype (bottom). *D*, Mammary tumors derived from MMTV/*rtTA* × tet-op/*PIK3CA*[H1047R] transgenic mice were transplanted into the mammary fat pad of athymic nude mice. Once tumors reached ≥250 mm³, mice were treated daily with vehicle or gefitinib (100 mg/kg orogastric gavage). Average tumor volume ±S.E. of six vehicle-treated and nine gefitinib-treated tumors is presented in mm³ (*p < 0.05 Student's t test). *E*, Tumor-bearing mice were treated for 4 days. 1 h after final treatment, tumors were harvested, and lysates prepared followed by immunoblot analyses. *F–G*, BT20 and SUM102 cells were cultured in starvation media with DMSO (D) or 1 μM Gefitinib, (G). Plates were fixed on days 0, 2, 4, and 6. Media and drugs were replenished every 3 days. Relative proliferation was assessed by SRB assay (*F*; average of six biological replicates ± S.E.). After 4 days of treatment, cell lysates were prepared for immunoblot analyses, *G*.

8/23 patients achieved a pathological complete response (pCR: no detectable tumor in the post-treatment mastectomy specimen). DNA was extracted from 19 available pretreatment biopsies (5 pCR, 14 nonpCR) and subjected to competitive allele-specific PCR to detect *PIK3CA* hot spot mutations. One of five tumors (20%) that achieved a pCR contained E545K *PIK3CA* whereas all nonresponsive tumors harbored wild-type *PIK3CA* (Chi-squared = 2.956 with one degree of freedom p = 0.0428, one tailed).

In another clinical trial evaluating chemotherapy (irinotecan + carboplatin) plus cetuximab in patients with metastatic TNBC (ClinicalTrials.gov #NCT00248287), one patient exhibited an exceptional clinical response. After 8 months of treatment, the primary breast tumor and pulmonary metastases responded completely. At this time, the patient underwent lumpectomy that showed no residual cancer in the breast; cetuximab alone

was continued. One year later a pulmonary mass recurred and was surgically resected, showing histology identical to the original cancer. The patient was rendered free of disease and continued on cetuximab treatment for 8 years with no evidence of recurrence. DNA from the primary breast tumor and the lung metastasis that recurred 8 months after the original diagnosis were extracted and subjected to targeted NGS of 3,769 exons of 236 oncogenes and tumor suppressors plus 47 introns of 19 genes frequently rearranged in cancer. Both lesions harbored the same *TP53* mutation (832C>T, p.P278S) and *MCL1* and *MYC* amplifications suggesting similar clonal origin of the primary tumor and the metastasis. However, an activating *PIK3CA* mutation (1258T>C, p.C420R) (33) found in the pretreatment breast cancer biopsy was undetectable in the recurrent lung metastasis. These data suggest that the *PIK3CA* mutant primary tumor was likely EGFR-dependent

and eliminated by treatment with cetuximab whereas the *PIK3CA* WT lung metastasis was not. Although limited, these clinical data are consistent with EGFR-dependent tumor cell proliferation induced by mutant *PIK3CA* that can be exploited with therapeutic intent.

The data above suggest *PIK3CA* mutant tumors depend, at least in part, on EGFR for their viability. To expand on this, we treated *PIK3CA* mutant BLBC cells and transgenic mouse mammary tumors driven by *PIK3CA*^{H1047R} (11) with the EGFR inhibitor gefitinib. Of note, cetuximab was not used because it does not recognize mouse EGFR. Murine mammary tumors driven by transgenic expression of *PIK3CA*^{H1047R} express higher levels of AREG mRNA and protein compared with transgenic mammary tumors driven by HER2 (supplemental Fig. S6A–S6B) (12). Importantly, these *PIK3CA*^{H1047R} tumors have been shown to cluster with transgenic mouse tumors with basal-like gene expression, such as C3-Tag (34). Gefitinib inhibited P-EGFR and P-ERK and delayed growth of *PIK3CA*^{H1047R} transgenic tumors (Fig. 6D–6E). Gefitinib also reduced the proliferation of *PIK3CA* mutant human BLBC BT20 and SUM102 cells and also reduced the phosphorylation of Akt and ERK (Fig. 6F–6G). These data suggest that blockade of EGFR is a therapeutic strategy which warrants further clinical investigation in BLBC with aberrant activation of PI3K.

DISCUSSION

Proteomic analysis of MCF10A cells identified a key role for secreted factors in growth factor-independent proliferation induced by *PIK3CA* hot spot mutations. A similar model which utilized microarray analyses focused on mutant *PIK3CA*-induced, NFκB-dependent cytokine production and STAT3 induction (35). In our studies, proliferation of WT cells was conferred by the media conditioned by *PIK3CA* mutant cells. Growth induced by media conditioned by *PIK3CA* mutant cells was insensitive to PI3K inhibitors, suggesting that these secreted factors operate independent of cell-intrinsic PI3K signaling. In addition, the cooperation between two secreted factors, fibronectin and AREG, in the induction of proliferation and ERK activation suggests that ECM molecules induced by mutant *PIK3CA* play a causative role in proliferation induced by growth factors such as AREG. This is consistent with other studies in which fibronectin and growth factors cooperate to induce activation of ERK and cell cycle entry (36) or in which AREG stimulates fibronectin expression (37). Because matrix stiffening by ECM crosslinking is itself tumor promoting (38), we speculate that the up-regulation of ECM molecules and the matrix crosslinking enzyme PXDN (39) are novel mechanisms of tumor promotion by mutant *PIK3CA*. Indeed, knockdown of some of these components, including laminins, THBS1 and PXDN, hindered the proliferation of *PIK3CA* mutant MCF10A and BLBC cell lines. PI3K activation was associated with increased exosome secretion, which could be because of the promotion of actin cytoskeletal rearrange-

ments, such as invadopodia formation by PI3K lipid products (30, 40). A phosphoproteomic and signaling network analysis of *PIK3CA* mutant MCF10A cells revealed novel substrates of Akt1, including cortactin, which was an important substrate for the enhanced migration induced by *PIK3CA* mutation (41). Because of the role of cortactin in invadopodia formation (42), and the association with invadopodia formation and exosome secretion (30), we speculate that the activation of cortactin in *PIK3CA* mutant cells was likely a critical aspect of the increased exosome secretion which we observed. Most of the secreted proteins identified in our LC-MS/MS analysis, including EGFR ligands and ECM molecules, were contained on exosomes, suggesting that a concerted secretion-proliferation/invasion program involving exosomes is induced by *PIK3CA* mutations.

The overexpression of EGFR in BLBC has been reported previously and our results suggest novel mechanisms by which EGFR is activated in BLBC with aberrant PI3K activity. Indeed, analysis of breast cancers performed by TCGA revealed that the basal-like subtype has the highest level of PI3K activity as inferred from RNA, protein and pathway activation scores (1). Further, PTPRF expression was markedly reduced in *PIK3CA* mutant cells and shRNA-mediated knockdown of PTPRF in *PIK3CA* WT cells resulted in EGFR activation as measured by P-EGFR levels. These results are consistent with studies showing an association between overexpression of miR-24, which down-regulates PTPRF, and concurrently enhanced EGFR activity (43). Laminin γ2, up-regulated by *PIK3CA* mutation, can be cleaved extracellularly, releasing EGF-like motifs also capable of activating EGFR (44), suggesting another potential mechanism by which EGFR-dependent proliferation could occur in *PIK3CA* mutant cells. Thus, multiple proteomic consequences of *PIK3CA* mutation (up-regulation of AREG, laminin γ2, and fibronectin and down-regulation of the PTPRF phosphatase) may all cooperate in the induction of EGFR/ERK signaling.

AREG overexpression was a mechanism by which *PIK3CA* mutant MCF10A cells induced EGFR activity and proliferation. Because activation of the oncogenic YAP transcription factor in MCF10A cells has been shown to induce AREG and paracrine proliferation (27), we examined whether induction of AREG was a "generic" mechanism by which cancer lesions activate growth factor-independent growth of MCF10A cells. However, *HRAS* mutant MCF10AT1 cells, which grow in the absence of exogenous growth factors, secreted far less AREG than *PIK3CA* mutant cells, were insensitive to AREG blockade and were unable to induce paracrine growth of WT cells. These results suggest not all oncogenes use AREG for growth factor-independent proliferation. High AREG mRNA levels in a breast cancer cell line gene expression data set (4) and AREG protein measured by ELISA (supplemental Fig. S3B–S3C) correlated with *PIK3CA* mutation status. In addition, MCF7, T47D, BT20, and SUM102 *PIK3CA* mutant cells, exhibited PI3K-dependent AREG expression, as has been

reported in RT4 bladder cancer cells (45). Our analysis of TCGA data and previous studies (18) categorize AREG as a nonbasal EGFR ligand, however, our ELISA data showed that AREG is also expressed in BLBC cells. Additionally, of the cell lines with highest levels of *AREG* mRNA, over half are basal-like, and the two cell lines with highest levels of *AREG*, SUM149, and HCC1954, are both basal-like and PTEN-deficient or P*IK3CA* mutant, respectively (4, 46). Further, SUM149 cells are dependent on AREG for proliferation in the absence of exogenous growth factors (47), similar to *PIK3CA* mutant MCF10A cells. Therefore, AREG appears to be a growth factor induced by PI3K activity in both luminal and basal-like cells as suggested by Kappler and colleagues (37).

Because EGFR is overexpressed in a cohort of TNBC, the majority of which exhibit basal-like gene expression, clinical trials of chemotherapy plus the EGFR antibody cetuximab have been conducted in patients with TNBC. In a randomized trial of cisplatin $\pm$ the EGFR antibody cetuximab, the combination induced a doubling of the overall clinical response rate compared with cisplatin alone (32). The modest clinical activity of EGFR inhibitors suggests the need of predictive biomarkers for patient selection, understanding mechanisms of EGFR pathway activation in TNBC and identification of the best combination of targeted therapies.

The results shown herein suggest that *AREG* is induced upon transformation by *PIK3CA* mutations, which can be reversed with inhibition of p110α. In addition, *PIK3CA* mutant BLBC cells and mouse transgenic basal-like mammary tumors driven by *PIK3CA*[H1047R] were sensitive to EGFR inhibition, suggesting that oncogenic activation of *PIK3CA* relies, in part, upon EGFR. We recognize, however, that in breast tumors with PI3K mutations, mutant *PIK3CA* is probably a more dominant oncogene and also a therapeutic target. Importantly, treatment with PI3K pathway inhibitors induces feedback up-regulation of several RTKs including the EGFR family (48–50). This compensatory up-regulation of RTKs limits the antitumor effect of PI3K inhibitors. Thus, we posit that the antitumor action of PI3K inhibitors in BLBC with PI3K mutations should be enhanced by cotreatment with EGFR inhibitors. This combination should blunt the feed-forward activation of AREG caused by aberrant PI3K activation described herein and the reactivation of RTKs that follows the inhibition of PI3K with targeted therapies.

Our studies have revealed pathways activated by mutant *PIK3CA* in BLBC which bear prognostic and therapeutic implications. The suite of proteins induced by mutant *PIK3CA* and identified by LC-MS/MS are associated with a poor prognosis in patients with BLBC and their down-regulation by siRNA reduced the proliferation of BLBC cell lines, suggesting these proteins as both markers of BLBC virulence and potential drug targets. The induction of AREG/EGFR by mutant *PIK3CA* and the evidence of clinical response to anti-EGFR therapies in patients with *PIK3CA* mutant BLBC warrant the inclusion of EGFR inhibitors in combination therapies against BLBC mutations in the PI3K pathway.

d To whom correspondence should be addressed: Division of Hematology-Oncology, Vanderbilt University, 2220 Pierce Avenue, 777 PRB, Nashville TN 37232-6307. Tel.: (615) 936 0381; Fax: (615) 343 0762; E-mail: carlos.arteaga@vanderbilt.edu.

e Current address: Kanagawa Cancer Center, Division of Cancer Cell Research, Yokohama, Japan.

REFERENCES

1. TCGA (2012) Comprehensive molecular portraits of human breast tumours. *Nature* **490,** 61–70
2. Debnath, J., and Brugge, J. S. (2005) Modeling glandular epithelial cancers in three-dimensional cultures. *Nat. Rev. Cancer* **5,** 675–688
3. Gustin, J. P., Karakas, B., Weiss, M. B., Abukhdeir, A. M., Lauring, J., Garay, J. P., Cosgrove, D., Tamaki, A., Konishi, H., Konishi, Y., Mohseni, M., Wang, G., Rosen, D. M., Denmeade, S. R., Higgins, M. J., Vitolo, M. I., Bachman, K. E., and Park, B. H. (2009) Knockin of mutant PIK3CA activates multiple oncogenic pathways. *Proc. Natl. Acad. Sci. U.S.A.* **106,** 2835–2840
4. Neve, R. M., Chin, K., Fridlyand, J., Yeh, J., Baehner, F. L., Fevr, T., Clark, L., Bayani, N., Coppe, J. P., Tong, F., Speed, T., Spellman, P. T., DeVries, S., Lapuk, A., Wang, N. J., Kuo, W. L., Stilwell, J. L., Pinkel, D., Albertson, D. G., Waldman, F. M., McCormick, F., Dickson, R. B., Johnson, M. D., Lippman, M., Ethier, S., Gazdar, A., and Gray, J. W. (2006) A collection of breast cancer cell lines for the study of functionally distinct cancer subtypes. *Cancer Cell* **10,** 515–527
5. Wang, H., Qian, W. J., Mottaz, H. M., Clauss, T. R., Anderson, D. J., Moore, R. J., Camp, D. G., 2nd, Khan, A. H., Sforza, D. M., Pallavicini, M., Smith, D. J., and Smith, R. D. (2005) Development and evaluation of a micro- and nanoscale proteomic sample preparation method. *J. Proteome Res.* **4,** 2397–2403
6. Cargile, B. J., Sevinsky, J. R., Essader, A. S., Stephenson, J. L., Jr., and Bundy, J. L. (2005) Immobilized pH gradient isoelectric focusing as a first-dimension separation in shotgun proteomics. *J. Biomol. Techn.* **16,** 181–189
7. Ma, Z. Q., Tabb, D. L., Burden, J., Chambers, M. C., Cox, M. B., Cantrell, M. J., Ham, A. J., Litton, M. D., Oreto, M. R., Schultz, W. C., Sobecki, S. M., Tsui, T. Y., Wernke, G. R., and Liebler, D. C. (2011) Supporting tool suite for production proteomics. *Bioinformatics* **27,** 3214–3215
8. Tabb, D. L., Fernando, C. G., and Chambers, M. C. (2007) MyriMatch: highly accurate tandem mass spectral peptide identification by multivariate hypergeometric analysis. *J. Proteome Res.* **6,** 654–661
9. Zhang, B., Chambers, M. C., and Tabb, D. L. (2007) Proteomic parsimony through bipartite graph analysis improves accuracy and transparency. *J. Proteome Res.* **6,** 3549–3557
10. Li, M., Gray, W., Zhang, H., Chung, C. H., Billheimer, D., Yarbrough, W. G., Liebler, D. C., Shyr, Y., and Slebos, R. J. (2010) Comparative shotgun proteomics using spectral count data and quasi-likelihood modeling. *J. Proteome Res.* **9,** 4295–4305
11. Liu, P., Cheng, H., Santiago, S., Raeder, M., Zhang, F., Isabella, A., Yang, J., Semaan, D. J., Chen, C., Fox, E. A., Gray, N. S., Monahan, J., Schlegel, R., Beroukhim, R., Mills, G. B., and Zhao, J. J. (2011) Oncogenic PIK3CA-driven mammary tumors frequently recur via PI3K path-

way-dependent and PI3K pathway-independent mechanisms. *Nat. Med.* **17,** 1116–1120

12. Hanker, A. B., Pfefferle, A. D., Balko, J. M., Kuba, M. G., Young, C. D., Sanchez, V., Sutton, C. R., Cheng, H., Perou, C. M., Zhao, J. J., Cook, R. S., and Arteaga, C. L. (2013) Mutant PIK3CA accelerates HER2-driven transgenic mammary tumors and induces resistance to combinations of antiHER2 therapies. *Proc. Natl. Acad. Sci. U.S.A.* **110,** 14372–14377

13. Wang, S. E., Xiang, B., Guix, M., Olivares, M. G., Parker, J., Chung, C. H., Pandiella, A., and Arteaga, C. L. (2008) Transforming growth factor beta engages TACE and ErbB3 to activate phosphatidylinositol-3 kinase/Akt in ErbB2-overexpressing breast cancer and desensitizes cells to trastuzumab. *Mol. Cell. Biol.* **28,** 5605–5620

14. Wang, X., Spandidos, A., Wang, H., and Seed, B. (2012) PrimerBank: a PCR primer database for quantitative gene expression analysis, 2012 update. *Nucleic Acids Res.* **40,** D1144–1149

15. Chang, J. T., and Nevins, J. R. (2006) GATHER: a systems approach to interpreting genomic signatures. *Bioinformatics* **22,** 2926–2933

16. Gyorffy, B., Lanczky, A., Eklund, A. C., Denkert, C., Budczies, J., Li, Q., and Szallasi, Z. (2010) An online survival analysis tool to rapidly assess the effect of 22,277 genes on breast cancer prognosis using microarray data of 1809 patients. *Breast Cancer Res. Treat.* **123,** 725–731

17. Gatza, M. L., Lucas, J. E., Barry, W. T., Kim, J. W., Wang, Q., Crawford, M. D., Datto, M. B., Kelley, M., Mathey-Prevot, B., Potti, A., and Nevins, J. R. (2010) A pathway-based classification of human breast cancer. *Proc. Natl. Acad. Sci. U.S.A.* **107,** 6994–6999

18. Hoadley, K. A., Weigman, V. J., Fan, C., Sawyer, L. R., He, X., Troester, M. A., Sartor, C. I., Rieger-House, T., Bernard, P. S., Carey, L. A., and Perou, C. M. (2007) EGFR associated expression profiles vary with breast tumor subtype. *BMC Genomics* **8,** 258

19. Hoadley, K. A., Yau, C., Wolf, D. M., Cherniack, A. D., Tamborero, D., Ng, S., Leiserson, M. D., Niu, B., McLellan, M. D., Uzunangelov, V., Zhang, J., Kandoth, C., Akbani, R., Shen, H., Omberg, L., Chu, A., Margolin, A. A., Van't Veer, L. J., Lopez-Bigas, N., Laird, P. W., Raphael, B. J., Ding, L., Robertson, A. G., Byers, L. A., Mills, G. B., Weinstein, J. N., Van Waes, C., Chen, Z., Collisson, E. A., Benz, C. C., Perou, C. M., and Stuart, J. M. (2014) Multiplatform analysis of 12 cancer types reveals molecular classification within and across tissues of origin. *Cell* **158,** 929–944

20. Dave, B., Granados-Principal, S., Zhu, R., Benz, S., Rabizadeh, S., Soon-Shiong, P., Yu, K., Shao, Z., Li, X., Gilcrease, M., Lai, Z., Chen, Y., Huang, T. H., Shen, H., Liu, X., Ferrari, M., Zhan, M., Wong, S. T., Kumaraswami, M., Mittal, V., Chen, X., Gross, S. S., and Chang, J. C. (2014) Targeting RPL39 and MLF2 reduce tumor initiation and metastasis in breast cancer by inhibiting nitric oxide synthase signaling. *Proc. Natl. Acad. Sci. U.S.A.* **111,** 8838–8843

21. Frampton, G. M., Fichtenholtz, A., Otto, G. A., Wang, K., Downing, S. R., He, J., Schnall-Levin, M., White, J., Sanford, E. M., An, P., Sun, J., Juhn, F., Brennan, K., Iwanik, K., Maillet, A., Buell, J., White, E., Zhao, M., Balasubramanian, S., Terzic, S., Richards, T., Banning, V., Garcia, L., Mahoney, K., Zwirko, Z., Donahue, A., Beltran, H., Mosquera, J. M., Rubin, M. A., Dogan, S., Hedvat, C. V., Berger, M. F., Pusztai, L., Lechner, M., Boshoff, C., Jarosz, M., Vietz, C., Parker, A., Miller, V. A., Ross, J. S., Curran, J., Cronin, M. T., Stephens, P. J., Lipson, D., and Yelensky, R. (2013) Development and validation of a clinical cancer genomic profiling test based on massively parallel DNA sequencing. *Nat. Biotechnol.* **31,** 1023–1031

22. Lipson, D., Capelletti, M., Yelensky, R., Otto, G., Parker, A., Jarosz, M., Curran, J. A., Balasubramanian, S., Bloom, T., Brennan, K. W., Donahue, A., Downing, S. R., Frampton, G. M., Garcia, L., Juhn, F., Mitchell, K. C., White, E., White, J., Zwirko, Z., Peretz, T., Nechushtan, H., Soussan-Gutman, L., Kim, J., Sasaki, H., Kim, H. R., Park, S. I., Ercan, D., Sheehan, C. E., Ross, J. S., Cronin, M. T., Janne, P. A., and Stephens, P. J. (2012) Identification of new ALK and RET gene fusions from colorectal and lung cancer biopsies. *Nat. Med.* **18,** 382–384

23. Soule, H. D., Maloney, T. M., Wolman, S. R., Peterson, W. D., Jr., Brenz, R., McGrath, C. M., Russo, J., Pauley, R. J., Jones, R. F., and Brooks, S. C. (1990) Isolation and characterization of a spontaneously immortalized human breast epithelial cell line, MCF-10. *Cancer Res.* **50,** 6075–6086

24. Yeh, T. C., Marsh, V., Bernat, B. A., Ballard, J., Colwell, H., Evans, R. J., Parry, J., Smith, D., Brandhuber, B. J., Gross, S., Marlow, A., Hurley, B., Lyssikatos, J., Lee, P. A., Winkler, J. D., Koch, K., and Wallace, E. (2007) Biological characterization of ARRY-142886 (AZD6244), a potent, highly selective mitogen-activated protein kinase kinase 1/2 inhibitor. *Clin. Cancer Res.* **13,** 1576–1583

25. Fritsch, C., Huang, A., Chatenay-Rivauday, C., Schnell, C., Reddy, A., Liu, M., Kauffmann, A., Guthy, D., Erdmann, D., De Pover, A., Furet, P., Gao, H., Ferretti, S., Wang, Y., Trappe, J., Brachmann, S. M., Maira, S. M., Wilson, C., Boehm, M., Garcia-Echeverria, C., Chene, P., Wiesmann, M., Cozens, R., Lehar, J., Schlegel, R., Caravatti, G., Hofmann, F., and Sellers, W. R. (2014) Characterization of the novel and specific PI3Kalpha inhibitor NVP-BYL719 and development of the patient stratification strategy for clinical trials. *Mol. Cancer Therapeut.* **13,** 1117–1129

26. Hirai, H., Sootome, H., Nakatsuru, Y., Miyama, K., Taguchi, S., Tsujioka, K., Ueno, Y., Hatch, H., Majumder, P. K., Pan, B. S., and Kotani, H. (2010) MK-2206, an allosteric Akt inhibitor, enhances antitumor efficacy by standard chemotherapeutic agents or molecular targeted drugs *in vitro* and *in vivo*. *Mol. Cancer Therapeut.* **9,** 1956–1967

27. Zhang, J., Ji, J. Y., Yu, M., Overholtzer, M., Smolen, G. A., Wang, R., Brugge, J. S., Dyson, N. J., and Haber, D. A. (2009) YAP-dependent induction of amphiregulin identifies a noncell-autonomous component of the Hippo pathway. *Nature cell biology* **11,** 1444–1450

28. Higginbotham, J. N., Demory Beckler, M., Gephart, J. D., Franklin, J. L., Bogatcheva, G., Kremers, G. J., Piston, D. W., Ayers, G. D., McConnell, R. E., Tyska, M. J., and Coffey, R. J. (2011) Amphiregulin exosomes increase cancer cell invasion. *Curr. Biol.* **21,** 779–786

29. Thery, C. (2011) Exosomes: secreted vesicles and intercellular communications. *F1000 Biol. Rep.* **3,** 15

30. Hoshino, D., Kirkbride, K. C., Costello, K., Clark, E. S., Sinha, S., Grega-Larson, N., Tyska, M. J., and Weaver, A. M. (2013) Exosome secretion is enhanced by invadopodia and drives invasive behavior. *Cell Rep.* **5,** 1159–1168

31. Blobel, C. P. (2005) ADAMs: key components in EGFR signalling and development. *Nat. Rev. Mol. Cell Biol.* **6,** 32–43

32. Baselga, J., Gomez, P., Greil, R., Braga, S., Climent, M. A., Wardley, A. M., Kaufman, B., Stemmer, S. M., Pego, A., Chan, A., Goeminne, J. C., Graas, M. P., Kennedy, M. J., Ciruelos Gil, E. M., Schneeweiss, A., Zubel, A., Groos, J., Melezinkova, H., and Awada, A. (2013) Randomized phase II study of the anti-epidermal growth factor receptor monoclonal antibody cetuximab with cisplatin versus cisplatin alone in patients with metastatic triple-negative breast cancer. *J. Clin. Oncol.* **31,** 2586–2592

33. Gymnopoulos, M., Elsliger, M. A., and Vogt, P. K. (2007) Rare cancer-specific mutations in PIK3CA show gain of function. *Proc. Natl. Acad. Sci. U.S.A.* **104,** 5569–5574

34. Young, C. D., Pfefferle, A. D., Owens, P., Kuba, M. G., Rexer, B. N., Balko, J. M., Sanchez, V., Cheng, H., Perou, C. M., Zhao, J. J., Cook, R. S., and Arteaga, C. L. (2013) Conditional loss of ErbB3 delays mammary gland hyperplasia induced by mutant PIK3CA without affecting mammary tumor latency, gene expression, or signaling. *Cancer Res.* **73,** 4075–4085

35. Hutti, J. E., Pfefferle, A. D., Russell, S. C., Sircar, M., Perou, C. M., and Baldwin, A. S. (2012) Oncogenic PI3K mutations lead to NF-kappaB-dependent cytokine expression following growth factor deprivation. *Cancer Res.* **72,** 3260–3269

36. Roovers, K., Davey, G., Zhu, X., Bottazzi, M. E., and Assoian, R. K. (1999) Alpha5beta1 integrin controls cyclin D1 expression by sustaining mitogen-activated protein kinase activity in growth factor-treated cells. *Mol. Biol. Cell* **10,** 3197–3204

37. Kappler, C. S., Guest, S. T., Irish, J. C., Garrett-Mayer, E., Kratche, Z., Wilson, R. C., and Ethier, S. P. (2014) Oncogenic signaling in amphiregulin and EGFR-expressing PTEN-null human breast cancer. *Molecular Oncology*, **9,** 527–543

38. Levental, K. R., Yu, H., Kass, L., Lakins, J. N., Egeblad, M., Erler, J. T., Fong, S. F., Csiszar, K., Giaccia, A., Weninger, W., Yamauchi, M., Gasser, D. L., and Weaver, V. M. (2009) Matrix crosslinking forces tumor progression by enhancing integrin signaling. *Cell* **139,** 891–906

39. Bae, Y. K., Kim, A., Kim, M. K., Choi, J. E., Kang, S. H., and Lee, S. J. (2013) Fibronectin expression in carcinoma cells correlates with tumor aggressiveness and poor clinical outcome in patients with invasive breast cancer. *Human Pathol.* **44,** 2028–2037

40. Carey, L. A., Rugo, H. S., Marcom, P. K., Mayer, E. L., Esteva, F. J., Ma, C. X., Liu, M. C., Storniolo, A. M., Rimawi, M. F., Forero-Torres, A., Wolff, A. C., Hobday, T. J., Ivanova, A., Chiu, W. K., Ferraro, M., Burrows, E., Bernard, P. S., Hoadley, K. A., Perou, C. M., and Winer, E. P. (2012) TBCRC 001: randomized phase II study of cetuximab in combination

with carboplatin in stage IV triple-negative breast cancer. *J. Clin. Oncol.* **30,** 2615–2623

41. Wu, X., Renuse, S., Sahasrabuddhe, N. A., Zahari, M. S., Chaerkady, R., Kim, M. S., Nirujogi, R. S., Mohseni, M., Kumar, P., Raju, R., Zhong, J., Yang, J., Neiswinger, J., Jeong, J. S., Newman, R., Powers, M. A., Somani, B. L., Gabrielson, E., Sukumar, S., Stearns, V., Qian, J., Zhu, H., Vogelstein, B., Park, B. H., and Pandey, A. (2014) Activation of diverse signaling pathways by oncogenic PIK3CA mutations. *Nat. Commun.* **5,** 4961

42. Clark, E. S., Whigham, A. S., Yarbrough, W. G., and Weaver, A. M. (2007) Cortactin is an essential regulator of matrix metalloproteinase secretion and extracellular matrix degradation in invadopodia. *Cancer Res.* **67,** 4227–4235

43. Du, W. W., Fang, L., Li, M., Yang, X., Liang, Y., Peng, C., Qian, W., O'Malley, Y. Q., Askeland, R. W., Sugg, S. L., Qian, J., Lin, J., Jiang, Z., Yee, A. J., Sefton, M., Deng, Z., Shan, S. W., Wang, C. H., and Yang, B. B. (2013) MicroRNA miR-24 enhances tumor invasion and metastasis by targeting PTPN9 and PTPRF to promote EGF signaling. *J. Cell Sci.* **126,** 1440–1453

44. Koshikawa, N., Minegishi, T., Sharabi, A., Quaranta, V., and Seiki, M. (2005) Membrane-type matrix metalloproteinase-1 (MT1-MMP) is a processing enzyme for human laminin gamma 2 chain. *J. Biol. Chem.* **280,** 88–93

45. Ornskov, D., Nexo, E., and Sorensen, B. S. (2007) Insulin induces a transcriptional activation of epiregulin, HB-EGF and amphiregulin, by a PI3K-dependent mechanism: identification of a specific insulin-responsive promoter element. *Biochem. Biophys. Res. Commun.* **354,** 885–891

46. Saal, L. H., Gruvberger-Saal, S. K., Persson, C., Lovgren, K., Jumppanen, M., Staaf, J., Jonsson, G., Pires, M. M., Maurer, M., Holm, K., Koujak, S., Subramaniyam, S., Vallon-Christersson, J., Olsson, H., Su, T., Memeo, L., Ludwig, T., Ethier, S. P., Krogh, M., Szabolcs, M., Murty, V. V., Isola, J., Hibshoosh, H., Parsons, R., and Borg, A. (2008) Recurrent gross mutations of the PTEN tumor suppressor gene in breast cancers with deficient DSB repair. *Nat. Genet.* **40,** 102–107

47. Willmarth, N. E., and Ethier, S. P. (2006) Autocrine and juxtacrine effects of amphiregulin on the proliferative, invasive, and migratory properties of normal and neoplastic human mammary epithelial cells. *J. Biol. Chem.* **281,** 37728–37737

48. Chandarlapaty, S., Sawai, A., Scaltriti, M., Rodrik-Outmezguine, V., Grbovic-Huezo, O., Serra, V., Majumder, P. K., Baselga, J., and Rosen, N. (2011) AKT inhibition relieves feedback suppression of receptor tyrosine kinase expression and activity. *Cancer Cell* **19,** 58–71

49. Chakrabarty, A., Sanchez, V., Kuba, M. G., Rinehart, C., and Arteaga, C. L. (2011) Breast Cancer Special Feature: Feedback upregulation of HER3 (ErbB3) expression and activity attenuates antitumor effect of PI3K inhibitors. *Proc. Natl. Acad. Sci. U.S.A.* **109,** 2718–2723

50. Fox, E. M., Kuba, M. G., Miller, T. W., Davies, B. R., and Arteaga, C. L. (2013) Autocrine IGF-I/insulin receptor axis compensates for inhibition of AKT in ER-positive breast cancer cells with resistance to estrogen deprivation. *Breast Cancer Res.* **15,** R55